AD-A109 604 UNIVERSIDAD AUTONOMA DE MADRID (SPAIN) DEPT OPTICA Y--ETC F/G 20/2
IMPURITY AGGREGATION PROCESSES AND MECHANICAL BEHAVIOR IN SOLID--ETC(U)
NOV 81 AFOSR-79-0115
UNCLASSIFIED EOARD-TR-82-2 NL

END
DATE
FILMED
2 82
DTIC

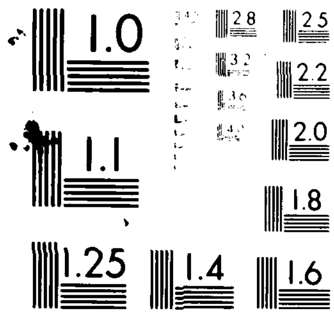

MICROCOPY RESOLUTION TEST CHART

AD A109604

REPORT DOCUMENTATION PAGE		READ INSTRUCTIONS BEFORE COMPLETING FORM
1. Report Number EOARD-TR-82-2	2. Govt Accession No. AD-A109 604	3. Recipient's Catalog Number
4. Title (and Subtitle) IMPURITY AGGREGATION PROCESSES AND MECHANICAL BEHAVIOR IN SOLID DIELECTRICS		5. Type of Report & Period Covered FINAL, 1 Sept. 79 31 Aug. 81
		6. Performing Org. Report Number
7. Author(s)		8. Contract or Grant Number AFOSR-79-0115
9. Performing Organization Name and Address Department Optica y Estructura de la Materia Universidad Autónoma de Madrid Cantoblanco. Madrid-34. Spain.		10. Program Element, Project, Task Area & Work Unit Numbers P.E.: 61102F Proj/Task: 2301/D1
11. Controlling Office Name and Address European Office of Aerospace Research & Development/CD Box 14 FPO New York 09510		12. Report Date 30 November 1981
		13. Number of Pages
14. Monitoring Agency Name and Address European Office of Aerospace Research & Development/CD Box 14 FPO New York 09510		15.

LEVEL II

16. & 17. Distribution Statement

Approved for public release; distribution unlimited.

DTIC ELECTE JAN 15 1982 D H

18. Supplementary Notes

19. Key Words

DIELECTRICS, AGGREGATION, IMPURITY, MECHANICAL.

20. Abstract

The aggregation and precipitation processes of divalent cation impurities in alkali halides have been followed by optical spectroscopy as well as ionic thermocurrent methods. In particular, a number of absorption and luminescence bands have been ascribed to well-defined precipitated phases. The influence of these precipitation processes on mechanical (yield-stress) behavior has been investigated and the different role of stable and metastable phases has been clearly differenciated.

412 134

FORM 1473

DTIC FILE COPY

82 01 11 161

This report has been reviewed by the EOARD Information Office and is releasable to the National Technical Information Service (NTIS). At NTIS it will be releasable to the general public, including foreign nations.

This technical report has been reviewed and is approved for publication.

OWEN MANCARELLA
Lt Colonel, USAF
Director, Aeronautical Systems

FOR THE COMMANDER

GORDON L. HERMANN
Lt Colonel, USAF
Deputy Commander

A

82 01 11 16[illegible]

EOARD-TR-82-2

Grant No. AFOSR-79-0115

IMPURITY AGGREGATION PROCESSES AND MECHANICAL BEHAVIOR IN SOLID DIELECTRICS

Fernando Agulló-López
Departamento de Optica y Estructura de la Materia
Universidad Autónoma de Madrid
Cantoblanco. Madrid-34. Spain.

30 November 1981

Final Report, 1 September 1979 - 31 August 1981

Approved for public release; distribution unlimited

Prepared for:

European Office of Aerospace Research and Development/AFSC

and

US Army Research and Standardization Group (Europe)

INDEX

1. INTRODUCTION

The main objectives of the present research project have been as follows:

i) To characterize the state of aggregation of divalent cation impurities in alkali halide single crystals by means of optical and EPR spectroscopy as well as ITC techniques. Most emphasis has been laid on optical spectroscopy (absorption and luminescence) including some Raman data.

ii) To elucidate the role of dislocations on aggregation and precipitation kinetics.

iii) To investigate the effect of the state of aggregation of the impurity on the mechanical strength of the crystal. One of the main aims is to try a correlation between the type of clusters and precipitates formed in the crystal and its yield-stress behavior.

2. OPTICAL SPECTROSCOPY TO STUDY PRECIPITATION OF DIVALENT CATION IMPURITIES

2.1 Lead Doped Crystals

Pb^{++} has absorption and luminescence spectra which are quite sensitive to the state of aggregation in the lattice (1,2). Consequently, it has been selected to optically monitor the clustering processes in alkali halides.

The absorption spectra of isolated Pb^{++} contains the so--called A, B, C and D bands in order of increasing energy. The A band is well separated from the other ones and can be conveniently studied. The peak position of the A band for several alkali halides is given in Table I. The luminescence spectra for isolated lead appears to be more complex. Main emission bands for excitation at the A band are also given in Table I.

Two different approaches have been followed to study the clustering and precipitation behaviour. In one type of experiment:

the aggregation processes have been monitored in several alkali halides doped with lead, by studying the change in the absorption and luminescence spectra of Pb^{++}. In particular, the ocurrence of new absorption bands around the A band, which may be associated to clusters and precipitates has been investigated. In other type of experiments, a small concentration of Pb^{++} ions has been introduced in a crystal containing a much higher concentration of another impurity M^{++}. It is expected that Pb^{++} may become incorporated into the clusters and precipitates of the majority impurity M^{++}. These Pb^{++} ions, placed in a different crystal environment, should give rise to new bands, providing information on the structure of the host clusters and precipitates.

The optical spectra were always taken at liquid nitrogen temperature (LNT) to improve the spectral resolution by using a conventional set-up. All doped crystals have been grown in our laboratory by the Czochralski method in an inert atmosphere, to avoid water contamination.

We will now consider separatedly the results obtained with the two experimental approaches.

2.1.1 Samples exclusively doped with lead ($AX:Pb^{++}$)

The following host alkali halides have been investigated: NaCl, KCl, KBr, KI and RbCl. Most complete data have been obtained for NaCl, KCl and KBr.

NaCl:Pb: The evolution of the absorption spectra at the A band region during ageing (isothermal annealing) has been followed at various temperatures. Figs. 1a and 1b show the results for NaCl:Pb aged at RT and 160°C respectively. At RT, additional bands develop on both sides of the A band (265 and 285 nm). The band at 285 nm approaches saturation at long annealing times. At 160°C, the same new bands grow initially with time. At longer times, the 285 nm band saturates and then decreases, whereas at the high-energy side a very prominent double band develops with peaks at 262 and 266 nm. Luminescence experiments to be described below have shown that this band is different from that occur

ring at RT. Figs. 2a and 2b show the growth of the various bands at RT and 160°C respectively. At 200°C the behaviour is similar to that at 160°C, although processes are faster.

The luminescence experiments permit to diferenciate among the bands appearing during RT or the initial stages of clustering at high-temperature and the double band typical of the late stage of ageing. The luminescence emissions of the intermediate bands (265 and 285 nm) lie in the 500-600 nm region, whereas the two component bands in the strongly aged sample (262 and 266 nm) show a well-defined emisssion at 430 nm, Fig. 3. It is to be remarked that this emission is the same observed when an as-grown sample is excited at the 265 nm band, previously attributed to $PbCl_2$ precipitates (3). On the other hand, the thermal annihilation of the two bands of the doublet occurs at the same temperature, Fig. 4, which also coincides with that for the 265 band of the $PbCl_2$ precipitates in the as-grown samples. It has been, therefore, concluded that the double band is, also, associated to $PbCl_2$ precipitates. The two component bands at 262 and 266 nm correspond to the splitted A transition of the Pb^{++} ions in the non-cubic crystal field.

The intermediate bands, which are the only ones appearing at RT, may be associated to the plate-zone precipitates already observed by Suzuki (4) in NaCl:Ca, although more work is necessary, for a definite assignement.

<u>KCl:Pb</u>: Similar ageing experiments have been performed for KCl:Pb. At RT no new bands develop. At 200°C, additional bands grow at both sides of the A band (264 and 280 nm), Fig. 5. It is noteworthy that the rate of growth of those bands very markedly depends on prior plastic straining, suggesting that dislocations may be involved as nucleation centers for the responsible phases. A comparison between the absorption spectra of unstrained and 3% strained samples after the same ageing time at 160°C is illustrated in Fig. 6.

The luminescence emission of the additional bands at 264 and 280 nm, consists of a main band at 550 nm. Some previous authors (5) have assigned the absorption and luminescence bands to Suzuki phase precipitates, although definite evidence is still lacking. Anyhow, at variance with NaCl:Pb, the presence of a band which could be attributed to $PbCl_2$ has not been detected in any of the experiments.

Raman spectra on samples presenting the 264 and 280 nm bands, have not shown any lines which may be attributed to Suzuki-phase (6) or $PbCl_2$ precipitates.

KBr:Pb: The A band of low doped and well quenched samples appears at 298 nm.

Ageing at RT or 100°C do not induce the occurrence of new bands. On the other hand, at 200°C, additional absorption bands at 307 and 323 nm are observed for concentrations ≥30 ppm, Fig. 7. These bands thermally disappear at temperatures ~300°C. For 450°C ageing, a well-resolved band at 265 nm grows, whereas those appearing at the lower temperatures are obviously abbsent.

Luminescence experiments will be performed in the future to clarify the origin of the various absorption bands.

RbCl:Pb and KI:Pb: For these materials, the experimental study has been less detailed.

In the case of RbCl:Pb,new bands appear on ageing, which depend on ageing temperature, Fig. 8.

For KI:Pb, several absorption bands develop during ageing treatments. Due to the highly higroscopic behavior of this material, the possible role of humidity in the optical spectra should be elucidated, before any meaningful conclusion can be obtained from the data.

2.1.2 Double Doped Samples ($AX:M^{++}:Pb^{++}$)

A small concentration (~10 ppm) of Pb^{++} has been introduced during growth in NaCl, together with a much higher concentra

tion (~300 ppm) of another divalent cation impurity M^{++} (M^{++}= Cd, Sr, Ca, Ba, Mg and Mn). The Pb^{++} ions are expected to monitor optically the clustering behavior of the major impurity M^{++}.

Fig. 9 shows the absorption spectra at LNT for as-grown samples of NaCl:Cd:Pb, NaCl:Ca:Pb and NaCl:Sr:Pb. For the three systems, the absorption spectra after quenching involve exclusively the typical A band of Pb^{++} at 272 nm. The as-grown samples show new well-defined bands at 284 nm for NaCl:Cd:Pb, 249 nm for NaCl:Sr:Pb and 258 nm for NaCl:Ca:Pb. In order to ascertain that these bands are, indeed, associated to lead, isothermal ageing treatments as well as thermal annihilation and luminescence experiments have been performed on them.

NaCl:Sr:Pb: This has been the system more thoroughly investigated. Fig. 10 shows absorption spectra after various ageing times at RT. An additional band grows at ~285 nm, between the A band and that appearing at 249 nm in the as-grown samples. In Fig. 11 similar data for 160°C ageing are displayed. Here the 255 nm band grows initially and then decreases in the benefit of the 249 nm band, which becomes prominent after long ageing times. The detailed kinetics of growth for the various bands is given in Figs. 12 and 13.

The thermal annihilation behavior of the various bands is shown in Fig. 14. Luminescence experiments have shown that the 255 nm band is made up of two different components at 255 nm and 260 nm, since their emissions are clearly different, Fig. 15. The emission band at 290 nm obtained for excitation at the 249 nm band is illustrated in Fig. 16, together with the excitation spectrum for the emission (see inset).

Comparison of these data with previous work (7,8,9) on NaCl:Sr, has led to the following conclusions:

a) The 249 nm band is associated to Pb^{++} embedded in $SrCl_2$ precipitates.

b) The 255 nm and 260 nm bands should correspond to Pb^{++} in

intermediate metastable phases in the formation of the $SrCl_2$ precipitates.

NaCl:Cd:Pb: Ageing at RT induces the growth of the absorption band at 284 nm appearing in the as-grown samples, Fig. 17. It presents a luminescence emission at 610 nm, and annihilates at ~90, Fig. 18. Complementary X-ray difraction experiments have revealed that in as-grown samples two phases are present. The Suzuki phase and the $2NaCl:Cl_2Cd$ (hexagonal) one, this being much more intense. This hexagonal phase disappears above ~150°C. On the other hand, previous X-ray data (10) have indicated that the Suzuki-phase annihilates at ~400°C (at higher concentrations).

In base to the available evidence the following temptative proposal is advanced:

The 284 nm band is ascribed to Pb^{++} embedded into the hexagonal phase.

NaCl:Ca:Pb: This system appears particularly complex. For as-grown samples, a prominent absorption band at 258 nm is observed, together with some indication of the A band, (see Fig. 9). The emission for excitation at 258 nm consists of a main band peaked at 340 nm.

During RT ageing (after quenching), the absorption spectrum approaches that of the as-grown samples. Two clear emissions appear at 340 nm and 365 nm, which are excited at 255 nm and 265 nm within the absorption band at 258 nm.

For samples aged at 200°C, a final absorption spectrum develops with a double band at 262-266 nm, Fig. 19, yielding intense emission at 290 nm.

It has been concluded that the double absorption band (262-266 nm) corresponds to Pb^{++} embedded in $CaCl_2$ precipitates, which have been shown (11) to form during high temperature ageing. The bands observed during RT ageing may correspond to intermediate phases in the formation of the $CaCl_2$ precipitates, such as the plate-zones found by X-ray diffraction (4).

2.2 Europium Doped Crystals

Since the end of the last reporting period a number of experiments have been performed on NaCl:Sr:Eu, where Eu^{++} is used as an optical probe to monitor the clustering behavior of Sr. Europium may be an alternative to lead in the optical study of clustering processes.

The observed optical spectra of divalent europium in alkali halides consists in the UV range of two broad bands which have been interpreted as transitions from the lowest Stark component of the $4f^7(^8S)$ ground state of Eu^{+2} to the t_{2g} and e_g components of the $4f^6 5d$ configuration (12). The separation between them is due to the 10 Dq splitting of the 5d orbitals by the crystal field. Recently, the optical spectrum of Eu^{++} has been shown to be quite sensitive to its state of aggregation (13). The absorption spectra for quenched and as-grown NaCl:Eu are given in Fig. 20.

<u>NaCl:Sr:Eu</u>: After quenching, the absorption (excitation) and emission spectra of NaCl:Sr:Eu are as for Eu^{++} dissolved in NaCl. For as-grown samples, the luminescence emission lies at 407 nm, which is close to that for $EuCl_2$. Also, the 10 Dq inferred from the excitation spectrum is very similar to that of Eu^{++} in $EuCl_2$. As a temptative proposal, the spectrum of as-grown samples is attributed to Eu^{++} in $SrCl_2$ precipitates.

More work is needed to get a more complete picture of Sr clustering by using Eu as optical probe, although the obtained data are very promising.

2.3 Conclusions

It has been clearly shown in this work that Pb is a very useful optical probe to follow clustering processes in alkali halides and identify some of the precipitates formed. In fact, well-defined additional absorption and luminescence bands develop on ageing and some of them have been ascribed to specific types of precipitates. Europium is also a very promising probe

to study precipitation, although more work is needed for a thorough evaluation of its usefulness. One of the advantages of europium lies in the use of EPR techniques in parallel with optical measurements to determine the structure of aggregates and precipitates.

Raman spectroscopy was shown to be an adequate tool for identification of precipitates (5). However in the present work, the Raman spectra have not permitted unambiguous identification of precipitates.

3. ITC DATA

The ITC technique has been used to study: a) impurity-vacancy dipoles and their ageing behavior and b) the relaxation peak associated to precipitated phases.

In relation to point a), the ITC spectra of KI doped with Ca, Sr, Pb and Ba has been investigated to complete the available experimental information. A dominant peak at 200°K, has been found in all systems and attributed to free dipoles. Relaxation parameters have been obtained.

As to point b) the ITC spectra of KCl:Pb has been studied after suitable thermal treatments apparently leading to the formation of Suzuki-phase precipitates. For ageing at 200°C, single relaxation peak with maximum at T_m = 252°K has been observed, Fig. 21. At 150°C an additional peak appears together with that observed at the higher temperature, Fig. 22.

The occurrence of two relaxation peaks may allow for explaining the dependence of the temperature T_m for the maximum of the ITC band with polarization time and temperature. So far, a correlation of these ITC peaks with optical bands has not been succesful.

4. E.P.R. DATA

Some E.P.R. data have been taken on alkali halide crys-

tals doped with a small concentration of Mn^{++}, as a paramagnetic probe, together with a much higher concentration of another divalent impurity M^{++} (Ca, Cd, Pb). Although the E.P.R. spectra have been shown to be sensitive to the thermal or ageing treatments, no conclusion has been obtained because of experimental failure at the end of the first reporting period.

5. MECHANICAL DATA

5.1 Summary of available data:

It has been recently reported (14), that the hardening behaviour during thermal annealing after quenching is quite different for NaCl:Pb and KCl:Pb. In fact, the yield-stress of NaCl:Pb increases markedly with annealing time for concentrations ≥15 ppm, whereas for KCl:Pb it remains constant even for concentrations as high as 220 ppm. Furthermore, treatments apparently leading to Suzuki-phase precipitates in this material (15) do not induce, either, an observable change in yield-stress. This clear difference between both systems was interpreted in terms of a different aggregation behaviour of lead ions. Semicoherent precipitates seem to be rapidly formed for NaCl:Pb, and lead to the incoherent phase $PbCl_2$ during high-temperature annealing (16, 17, 18) whereas aggregates and coherent precipitates (presumably Suzuki-phase like) are induced during annealing of KCl:Pb (15). For both systems, the initial stages of aggregation (formation of dimers, trimers, etc) do not cause any extra-hardening effect with regard to the isolated dipoles.

In addition to the above mentioned data for NaCl:Pb and KCl:Pb, some interesting data have been, also, published for other systems on the effect of impurity aggregation on yield-stress (19, 20). Unfortunately, the available information is still very scarce and fragmentary. Moreover, the data have been usually discussed (21, 22) in terms of a simple aggregation model of dipoles into small aggregates (trimers, etc) and the formation of well-defined precipitated phases has been ignored. Consequent-

ly, the influence of impurity precipitation on yield-stress behaviour has not been so far adequately considered.

In this work, we have extended the same type of experiments reported in (1) , to other divalent-cation doped systems. The main emphasis has been laid on systems (e.g. NaCl:Cd and NaCl:Ca), where the aggregation and precipitation behaviour has been studied by other techniques (23, 24, 25, 26, 27) and a reasonable understanding of the precipitates formed during annealing is available. In fact, the main objectives of this work is to elucidate the correlation between the nature of those precipitates and their effect on the yield-stress of alkali halide crystals.

5.2 Experimental Procedures

The system investigated have included: NaCl doped with Ca, Sr, Mn and Cd, KCl with Pb and KBr with Sr and Pb. For all cases, concentrations in the crystal have been determined by atomic absorption spectrophotometry. The study has been performed for standard size samples (4x4x10 mm^3) as well as small-size samples (2x2x6 mm^3) for which quenching rates are higher. The results are similar, although the scatter of data-points is quite large for the latter case.

Quenching treatments were performed by heating the sample for 20 min. at 450°C and then dropping it onto a copper block. The efficiency of this quenching rate for small-size samples has been checked as follows: for NaCl:Mn the broad EPR signal for aggregated manganese is eliminated for concentrations $\leq$200 ppm; for NaCl:Pb the optical absorption bands associated to $PbCl_2$ precipitates disappear for concentrations ~60 ppm and the ITC spectra consist of the single band corresponding to isolated dipoles for this concentrations. Anyhow, the situation for other systems and concentrations will depend on the detailed shape of the TTT diagrams and a definite prediction cannot be advanced, because perhaps for the higher concentrations the hardness after quenching cannot correspond with that due to isolated dipoles.

Isothermal annealing treatments were carried out in the temperature range 20-200°C. Mechanical testing was always carried out at room-temperature (RT), in an Instron testing machine. Stress-strain curves had in all cases the typical shape (28, 29). Macroscopic yield-stress values were determined by the intersection of the extrapolation of the easy-glide stage with the linear elastic region.

5.3 Results

First, it has been ascertained that for low enough concentrations, below a certain threshold depending on the material, all systems show a yield-stress which is independent of annealing time for all temperatures within the covered range. This is illustrated in Fig. 23 for NaCl:Mn (58 ppm) annealed at RT, where the evolution of the yield-stress with time is compared with the decrease in dipole-concentration as inferred from the EPR spectra. In the inset of that figure, the dependence of yield stress with annealing time at RT, 100 and 200°C for other systems (NaCl:Ca, KBr:Sr, NaCl:Cd and KBr:Pb) is included. This result confirms that the formation of the first aggregates (dimers, trimers) from the I-V dipoles does not modify the yield-stress of the crystal with regard to the isolated dipoles, as concluded in previous work (14).

For higher concentrations, where some type of precipitation is involved, the experimental data indicate that two opposite behaviours are found, depending on crystal systems:

A. NaCl:Cd, NaCl:Mn, KCl:Pb, KBr:Pb and KBr:Sr

For NaCl:Cd, where Suzuki-phase precipitates are unequivocally formed, the dependence of yield-stress on annealing time is given in Figs. 24 and 25. Fig. 24 shows the data corresponding to RT annealing and Fig. 25 those for samples annealed at 200°C. At RT, the yield-stress remains constant or perhaps experiences a slight initial increase with time for the lower concentrations (37 ppm), whereas for the higher concentrations it

shows a definite decrease during the initial stages of annealing (~10 hrs.). For longer annealing times, the yield-stress reaches a steady value in all cases. At 200°C, the situation is somewhat similar. Except for the lowest concentration, where the yield--stress is basically constant during annealing, a marked initial softening of the crystal is observed, until a final steady value of yield stress is found, as for the RT case. The amount of softening is much higher for 200°C than for RT annealing. For 100°C annealing the observed behaviour is intermediate between that described for RT and 200°C.

The same basic behaviour is found for other systems: KBr:Pb KBr:Sr and NaCl:Mn. Data on the evolution of the yield-stress with annealing time for KBr:Sr, containing various amounts of Sr, are shown in Fig. 26 and 27, corresponding to RT and 200°C annealing respectively. The results are quite similar to those described above for NaCl:Cd, although the decrease in yield-stress is,here, much more pronounced. A comparative plot of the effect of 200°C annealing on NaCl:Cd, KBr:Sr, KBr:Pb and NaCl:Mn crystals, with similar doping levels, is given in Fig. 28. The "softening" effect is particularly small for NaCl:Mn which also presents some peculiar behaviour at 100°C, where some initial softening, followed by hardening has been observed. More work should be necessary on this system to clarify its behaviour. Anyhow, efficient migration of Mn to the crystal surface has been reported during heating (30) that may interfere with the aggregation process and be responsible for the complex yield-stress behaviour.

For KCl:Pb, a detailed comparison can be made between the mechanical data and the evolution of the optical absorption spectra. As shown in Fig. 29, the yield-stress is constant during 200°C annealing whereas an absorption band at 280 nm grows steadily with time at the cost of the A band of Pb^{++}. At the same time, lead-vacancy dipoles decay with time as revealed by dielectric loss and ITC techniques on similarly doped samples (31). In fact, the additional optical bands have been associated to Suzuki-phase precipitates (32), although direct evidence for this

particular structure is not yet available.

For lead concentrations much higher (~3600 ppm) than those used previously, the yield-stress decreases with annealing time as commented above for NaCl:Cd, NaCl:Mn, KBr:Sr and KBr:Pb.

B. NaCl:Ca, NaCl:Sr, NaCl:Pb

The data obtained for NaCl:Ca, NaCl:Sr and NaCl:Pb, show an opposite behaviour to that corresponding to the materials included in section A. Fig. 30 illustrates the evolution of yield-stress with annealing time at 100°C for Nacl:Ca crystals, containing various amounts of Ca. It is clear that, now, a very marked hardening is obtained during annealing, for concentrations above a certain threshold. Comparative data for NaCl:Pb, NaCl:Sr and NaCl:Ca are given in Fig. 31. At higher temperatures, the annealing-induced saturation hardening becomes smaller as reported for NaCl:Pb. Data for NaCl:Sr are shown in Fig. 32. Above 175°C, practically no annealing-induced hardening is observed. For NaCl:Pb, the optical data described in section 2.1.1 can be now compared with the yield-stress data. Specifically the evolution of the yield-stress with time has been correlated with the growth of the optical bands developed during isothermal ageing. Fig. 33 shows the data for RT ageing and Fig. 34 those for 200°C ageing. At RT, only the intermediate band (286 nm) develops but not that one associated to $PbCl_2$. The yield-stress increases in good correlation with the growth of that 286 nm optical band. At 200°C, the initial rapid hardening is also associated to the growth of this intermediate band. For longer annealing times, where the 286 nm band decays in the benefit of that of $PbCl_2$, a clear decrease in yield-stress is observed.

5.4 Conclusions

Although it is not possible to give a detailed picture of the hardening (or softening) mechanisms operating in the various systems, some general conclusions can be inferred from the data:

a) The formation of small aggregates (dimers, trimers) from the isolated I-V dipoles does not induce any change in yield--stress for all the investigated systems. This conclusions is in accordance with that reported by Dryden et al. (19).

On the other hand, the changes in yield-stress observed by these authors for NaCl:Ca and LiF.Mg and attributed to the formation of larger aggregates are very likely related to the occurrence of precipitation processes as discussed below.

The constancy of the yield-stress, regardless of whether dipoles are isolated or forming small aggregates appears more consistent with a Snoek-type (33) than with a Fleischer hardening mechanism (34). In fact, the latter model would imply a yield-stress markedly dependent on aggregate configuration because of the differences in the associated stress-field, particularly its axiality.

b) For systems such as Nacl:Cd, where Suzuki-phase precipitates are formed, a clear softening of the material is observed during annealing for concentrations above a certain threshold. This behaviour could be attributed to the fact that these precipitates retain a high degree of coherence with the host lattice. In fact, one should presumably attribute the observed decrease in yield-stress to the increase in the interphase area between the precipitate and the crystal host associated to the cutting of the precipitates by the moving dislocations (35). This mechanism predicts a yield-stress value which decreases on increasing precipitate size, and consequently during annealing time. The amount of softening increases with annealing temperature, suggesting that the final precipitate size is correspondingly larger.

For the other systems where softening has been also observed, the simple criterion advanced by Sors and Lilley (36) suggests that Suzuki-phase precipitates are also expected since all $r_{++}/r_{+} \leq 1.2$, r_{++} and r_{+} respectively being the impurity and host cation radii.

In summary, the softening appears to be a general effect

associated to the Suzuki-phase or similarly coherent precipitates.

c) For systems, such as NaCl:Ca, NaCl:Sr and NaCl:Pb, where the stable dihalide phase has been reported to occur, a definite hardening is observed at not high annealing temperatures (≤150°C for NaCl:Pb and ≤100°C for NaCl:Ca and NaCl:Sr). However, the new data on NaCl:Pb unequivocally show that the hardening observed at these lower temperatures is not associated to the stable but to some intermediate phases. The same conclusion would apply to NaCl:Ca, where X-ray studies have revealed that the phases formed below ~100°C, correspond to small plate-like structures, called the plate-zones, parallel to {111} and {310} planes of the matrix lattice (10, 24). These plate-zones posses a stoichiometry similar to that of $CaCl_2$, although retaining some degree of coherency with the matrix. At higher temperatures, the plate-zones (specifically the {111}) turn into the incoherent dihalide $CaCl_2$ phase. In both cases NaCl:Ca and NaCl:Pb, the coherency of the intermediate phases should diminish during annealing because of the increasing precipitate size. This accounts for the initial hardening observed in the curves of Figs. 6 and 9. On the other hand, the formation of the stable phase at longer annealing times is associated with a lower value of the yield-stress, which is particularly significant at the higher temperatures. This effect can be explained in terms of an Orowan-type mechanism for the overcoming of the incoherent dihalide precipitates by the moving dislocations (35).

Although the precipitation behaviour for NaCl:Sr is not so clearly established, the situation appears to be similar. In fact, intermediate rod-like precipitated phases have been reported during low temperature annealing, which develop into $SrCl_2$ at higher temperatures. Furthermore, some very recent results on NaCl:Eu show the same behaviour and have been explained with a similar scheme (13).

As a summary, the correlation between the kind of mechanical response, the ratio r_{++}/r_{+} and the type of final precipitate formed or expected can be easily visualized in Table II. One

may conclude that measurements of the variation of yield-stress with ageing time can be used to follow and qualitatively distinguish the type of precipitation behaviour in divalent cation doped alkali halides.

6. REFERENCES

1. J.S. Dryden and C.G. Harvey, J. Phys. C 2, 603 (1969).
2. J.L. Pascual, L. Arizmendi, F.Jaque and F. Agulló-López, J. Lumin. 17, 325 (1978).
3. J.L. Pascual, J.M. Cabrera and F. Agulló-López, Sol. Stat. Comm. 19, 917 (1976).
4. K. Suzuki, J. Phys. Soc. Japan 13, 179 (1958).
5. S. Benci, R. Capelletti, F. Fermi, M. Manfredi, J.Z. Damm and E. Mugenski, Phys. Stat. Sol. (b) 90, 657 (1978).
6. J.M. Calleja, A. Ruiz, F. Flores, V.R. Velasco and E. Lilley, J. Phys. Chem. Solids 41, 1367 (1980).
7. E. Laredo and E. Dartyge, Acta Cryst. A27, 353 (1971).
8. A.I. Sors and E. Lilley, Phys. Stat. Sol. (a) 32, 533 (1975).
9. N. Brown and I.M. Hoodless, J. Phys. Chem. Solids 28, 2297 (1967).
10. N. Bonanos and E. Lilley, Mat. Res. Bull. 14, 1609 (1979).
11. K. Suzuki, J. Phys. Soc. Japan 13, 179 (1959).
12. J. Hernández A., W.K. Cory and J. Rubio O., J. Chem. Phys. 72, 198 (1980).
13. F.J. López, H. Murrieta S., J. Hernández A., and J. Rubio O., Phys. Rev. B22, 6428 (1980).
14. J. García Solé, C. Zaldo and F. Agulló-López, Phil. Mag. A 41, 17 (1980).
15. R. Capelletti, A. Gainotti and L. Pareti, Proceedings of the Symposium on Thermal and Photostimulated Currents in Insulation, edited by D.M. Smith (The Electrochemical Society, 1976).

16. A. Bohum, J. Dolejsi, M. Simeckova and H. Svobodova, Z. Phys. 243, 34 (1971).

17. J.L. Pascual, J.M. Cabrera and F. Agulló-López, Sol. Stat. Comm. 19, 917 (1976).

18. L. Marculescu, Phys. Stat. Sol. (b) 80, 265 (1977).

19. J.S. Dryden, S. Morimoto and J.S. Cook, Phil. Mag. 12, 379 (1965).

20. W.G. Johnston, J. Appl. Phys. 33, 2050 (1962).

21. A.I. Sors and E. Lilley, Phys. Stat. Sol. (a) 32, 533 (1975).

22. C.W.A. Neway, R.P. Harrison and P.L. Pratt, Proceedings of the British Ceramic Society 6, 305 (1966).

23. K. Suzuki, J. Phys. Soc. Japan 10, 794 (1955).

24. K. Suzuki, J. Phys. Soc. Japan 16, 67 (1961).

25. G.A. Andreev and V.A. Klimov, Sov. Phys. Solid State 16, 1926 (1975).

26. A.L. Guerrero, E.P. Butler and P.L. Pratt, Journal de Physique, Colloque C6, Supplement au n°7, 41, C6-363 (1980).

27. W. Spengler and R. Kaiser, Phys. Stat. Sol. (b) 66, 107 (1974).

28. R.W. Davidge and P.L. Pratt, Phys. Stat. Sol. 6, 759 (1964).

29. B.H. Kear, C.E. Silverstone and P.L. Pratt, Proceedings of the British Ceramic Society n° 6, 269 (1966).

30. E. Pedrero, T. Ocaña, A. Gómez and M. José Yacaman, Thin Solid Films 27, 149 (1975).

31. W.C. Collins and J.H. Crawford, J. Phys. Rev. 4B, 3745 (1971).

32. P.G. Bertoldi, R. Capelletti, F. Fermi, M. Manfredi and V.J. Graveris, J. de Physique, Colloque C6, n° 7, 367 (1980).

33. P.L. Pratt, R. Cheng and C. Newey, Appl. Phys. Let. 3, 83 (1963).

34. R.L. Fleischer, Acta Metallurgica 9, 996 (1961).

35. P. Haasen, Chapter 14 in Physical Metallurgy, Cambridge University Press (1978).

36. A. Sors and E. Lilley, Phys. Stat. Sol. (a) 27, 469 (1975).

7. POSTGRADUATE STUDENTS SUPPORTED BY THE GRANT

- Carlos Zaldo Luezas, from 30/9/79 to 31/12/80.
- José Luis Martínez Peña, from 1/1/81 to 30/9/81.

8. PUBLICATIONS

1. "Pb^{++} as an optical probe to investigate clustering processes of M^{++} in alkali halides", J. García Solé, C. Zaldo and F. Agulló-López, to be published in J. Lumin.
2. "Dielectric relaxation of impurity-vacancy complexes in doped KI", F. Cussó and F. Jaque, to be published in Cryst. Latt. Def.
3. "Optical spectroscopy of lead in NaCl:Sr crystals", J. García Solé, C. Zaldo and F. Agulló-López, to be published in Phys. Rev.
4. "Mechanical strengthening and impurity precipitation behavior for divalent cation doped alkali halides", C. Zaldo, J. García Solé and F. Agulló-López, to be published in J. Mat. Science.
5. "Study of the precipitation behavior of NaCl:Pb and KCl:Pb by optical spectroscopy", C. Zaldo, J. García Solé and F. Agulló-López, submitted to J. Phys. Chem. Solids.
6. Manuscript in preparation on "Optical spectroscopy of NaCl:Sr:Eu", to be submitted to Phys. Rev.
7. Manuscript in preparation on "Study of cadmium precipitation in NaCl, by using Pb as an optical probe"

9. SCIENTIFIC MEETINGS

1. Communication (accepted) to the Sixth European Crystallographic Meeting, Barcelona, Spain. July 1980. "Optical spectroscopy and mechanical testing to investigate clustering and

precipitation in alkali halide crystals".

2. Abstract presented at the 1981 International Conference on Luminescence, Berlin (West), 20-24 July. "Pb^{++} as an optical probe to investigate clustering processes of M^{++} in alkali halides".

3. The same abstract presented at the meeting of the European Section of the Electrochemical Society at Bellevue Laboratories (Paris, Francia).

4. Abstract presented at the 4th meeting of the Spanish Solid State Physics Group.

TABLE I

Wavelength location (nm) of A absorption and emission bands at LNT

Material	Absorption	Luminescence
NaCl	273	310, 380
KCl	272	345, 420
KBr	298	365, 470
KI	351	397

TABLE II

Material	Mechanical behaviour (above threshold concentration)	Ratio r_{++}/r_{+}	Type of precipitate
NaCl:Mn	Softening	0.84	Suzuki-phase (1)
KBr:Sr	Softening	0.85	------
KCl:Pb	Softening	0.90	Suzuki-phase? (3)
KBr:Pb	Softening	0.90	------
NaCl:Cd	Softening	1.02	Suzuki-phase (2)
NaCl:Ca	Hardening	1.04	Dihalide (4)
NaCl:Sr	Hardening	1.19	Dihalide (5)
NaCl:Pb	Hardening	1.26	Dihalide (6)

(1) J.A. Chapman and E. Lilley, J. Mat. Science 10, 1154 (1975); D.L. Kirk, A.R. Kahn and P.L. Pratt, J. Phys. D.: Appl. Phys. 8, 2013 (1975).

(2) K. Suzuki, J. Phys. Soc. Japan 16, 67 (1961).

(3) R. Capelletti, A. Gainotti, L. Pareti, Proceedings of the Symposium on thermal and photostimulated currents in insulators; edited by D.M. Smith (The Electrochemical Society, 1976).

(4) K. Suzuki, J. Phys. Soc. Japan 10, 794 (1955).

(5) A.I. Sors and E. Lilley, Phys. Stat. Sol. (a) 32, 533 (1975); E. Laredo and E. Dartyge, J. Chem. Phys. 53, 2214 (1970).

(6) A. Bohum, J. Dolejsi, M. Simeckova and [illegible], Z. Phys. 243, 244 (1971); J.L. Pascual, J.M. Cabrera and F. Agulló-López, Solid State Comm. 19, 917 (1976).

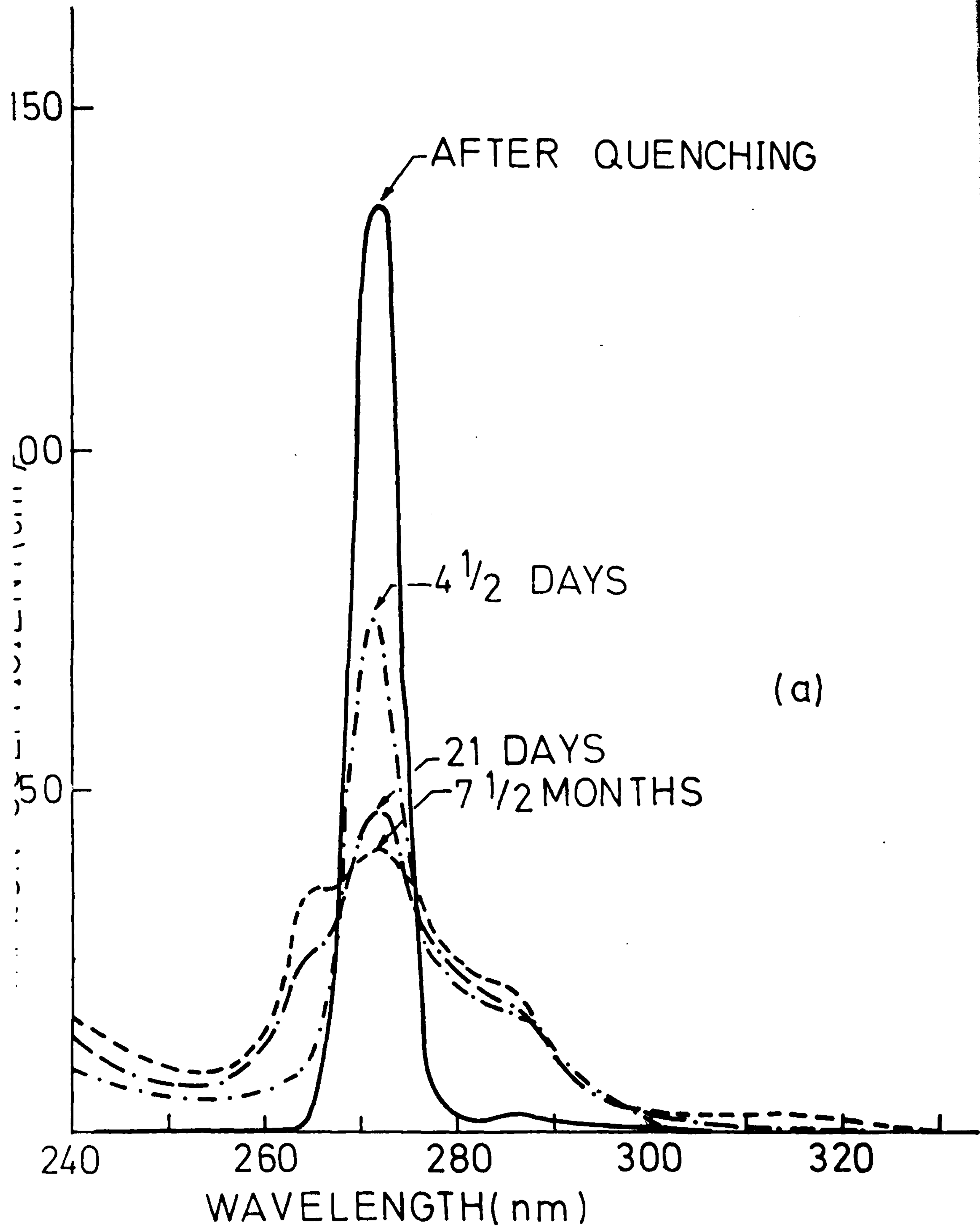
150
00
50
AFTER QUENCHING
4 1/2 DAYS
(a)
21 DAYS
7 1/2 MONTHS
240
260
280
300
320
WAVELENGTH(nm)

FIG. 1(A)

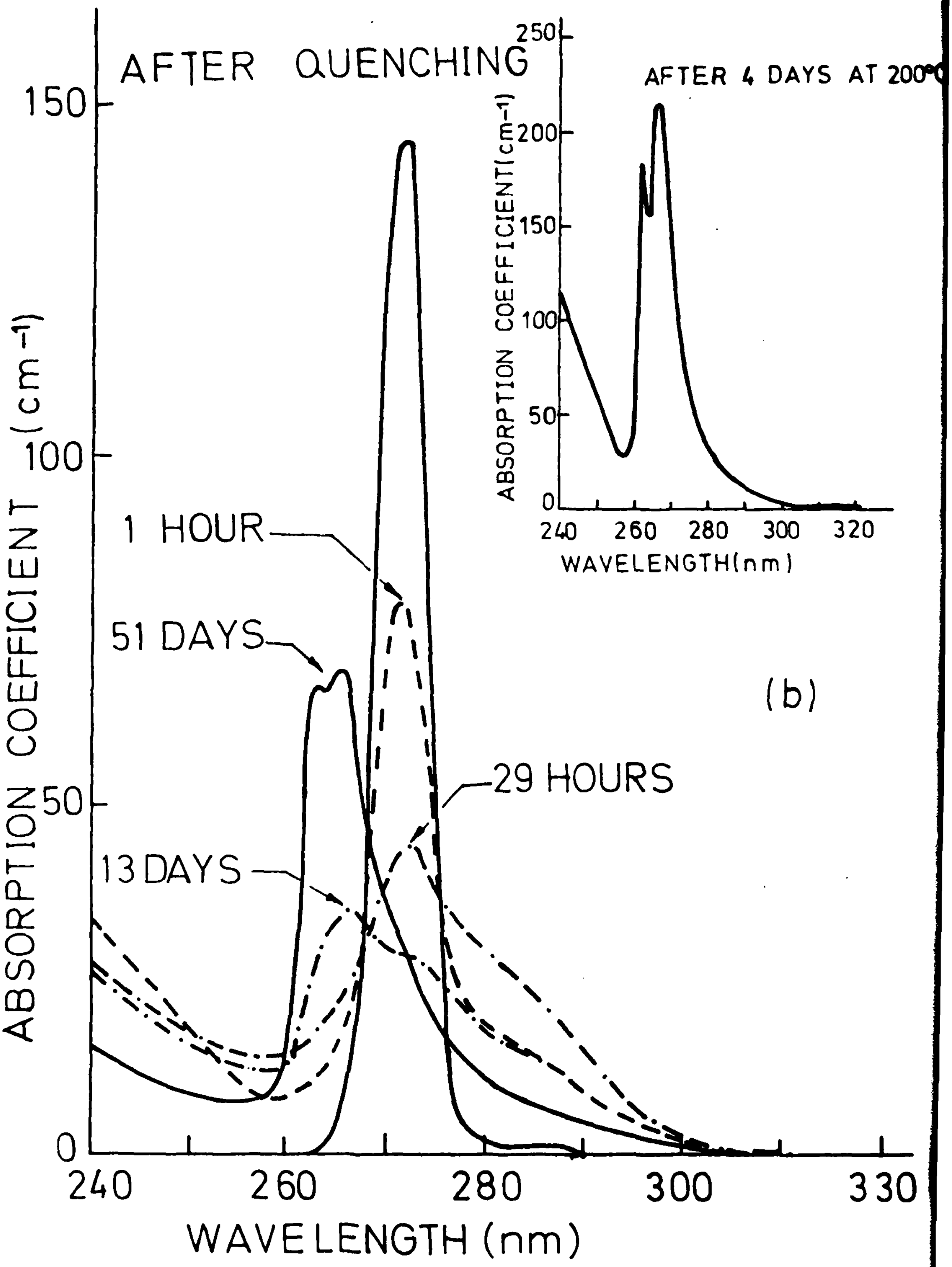
AFTER QUENCHING
150
100
50
0
ABSORPTION COEFFICIENT (cm-1)
1 HOUR
51 DAYS
29 HOURS
13 DAYS
(b)
240
260
280
300
330
WAVELENGTH (nm)
AFTER 4 DAYS AT 200°C
250
200
150
100
50
0
ABSORPTION COEFFICIENT(cm-1)
240
260
280
300
320
WAVELENGTH(nm)

FIG. 1(B)

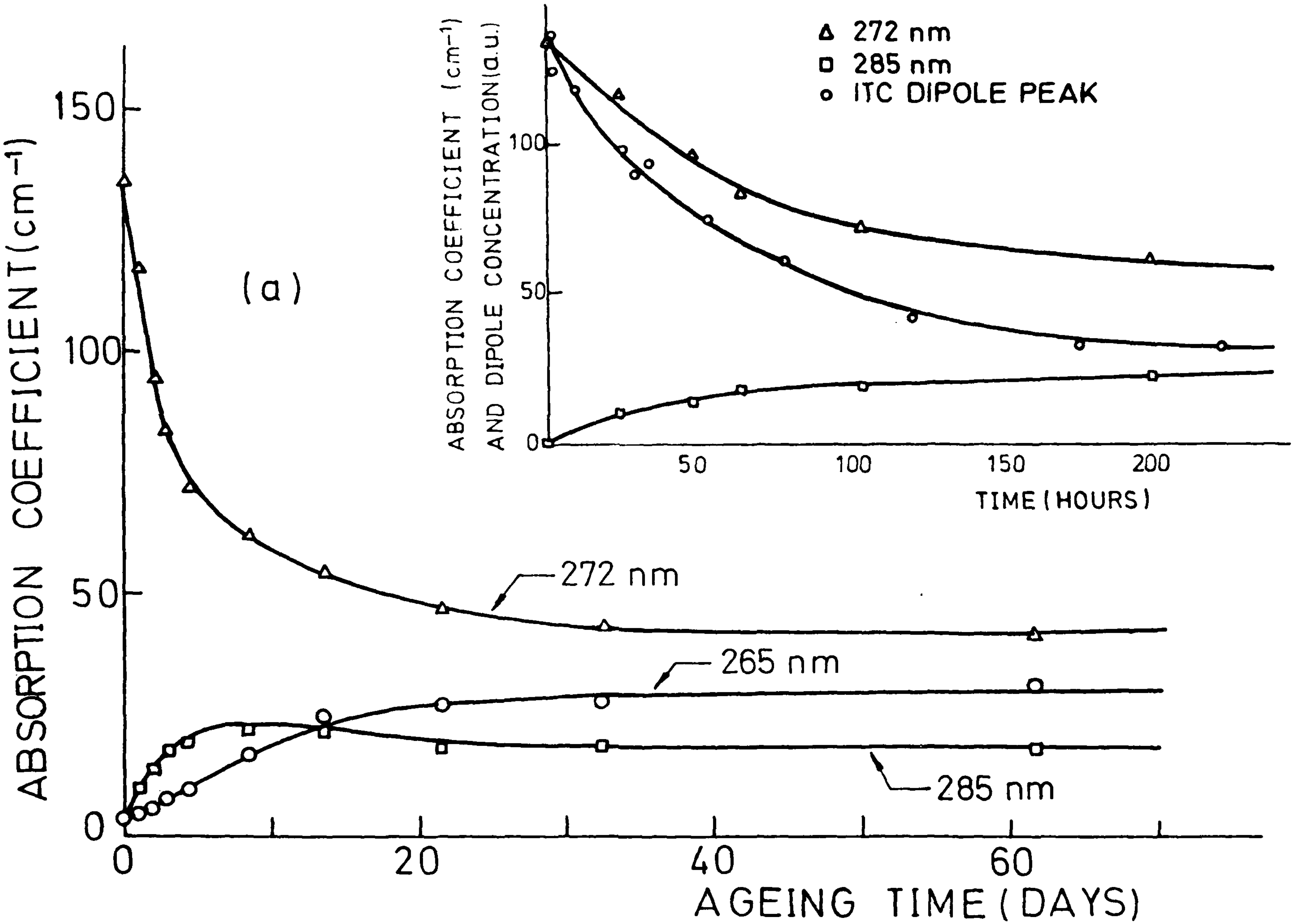

(a)
ABSORPTION COEFFICIENT (cm-1)
150
100
50
0
0
20
40
60
AGEING TIME (DAYS)
272 nm
265 nm
285 nm
272 nm
285 nm
ITC DIPOLE PEAK
ABSORPTION COEFFICIENT (cm-1)
AND DIPOLE CONCENTRATION (a.u.)
100
50
0
50
100
150
200
TIME (HOURS)

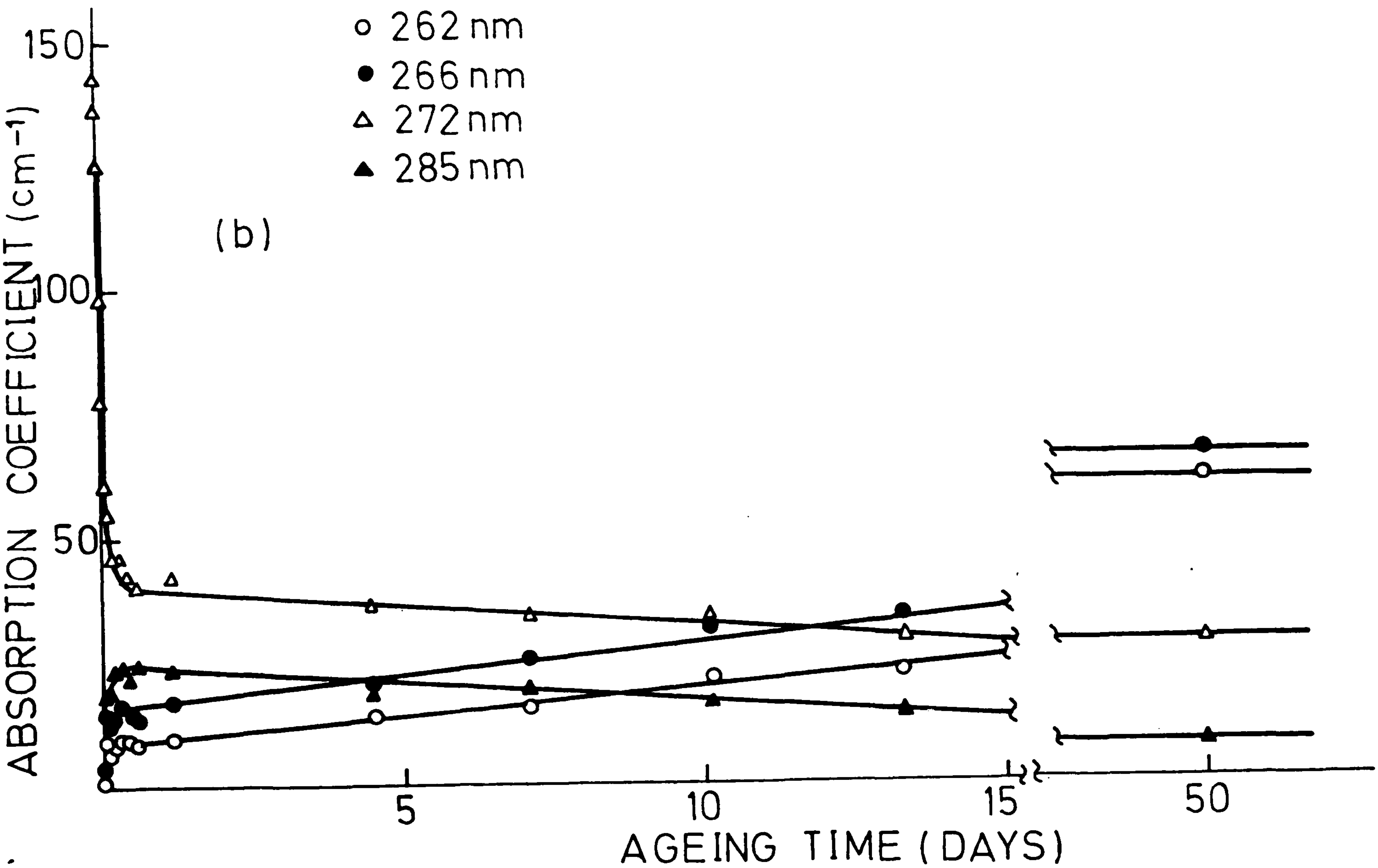

○ 262 nm
● 266 nm
△ 272 nm
▲ 285 nm
(b)
150
100
50
ABSORPTION COEFFICIENT (cm-1)
5
10
15
50
AGEING TIME (DAYS)

FIG. 2(B)

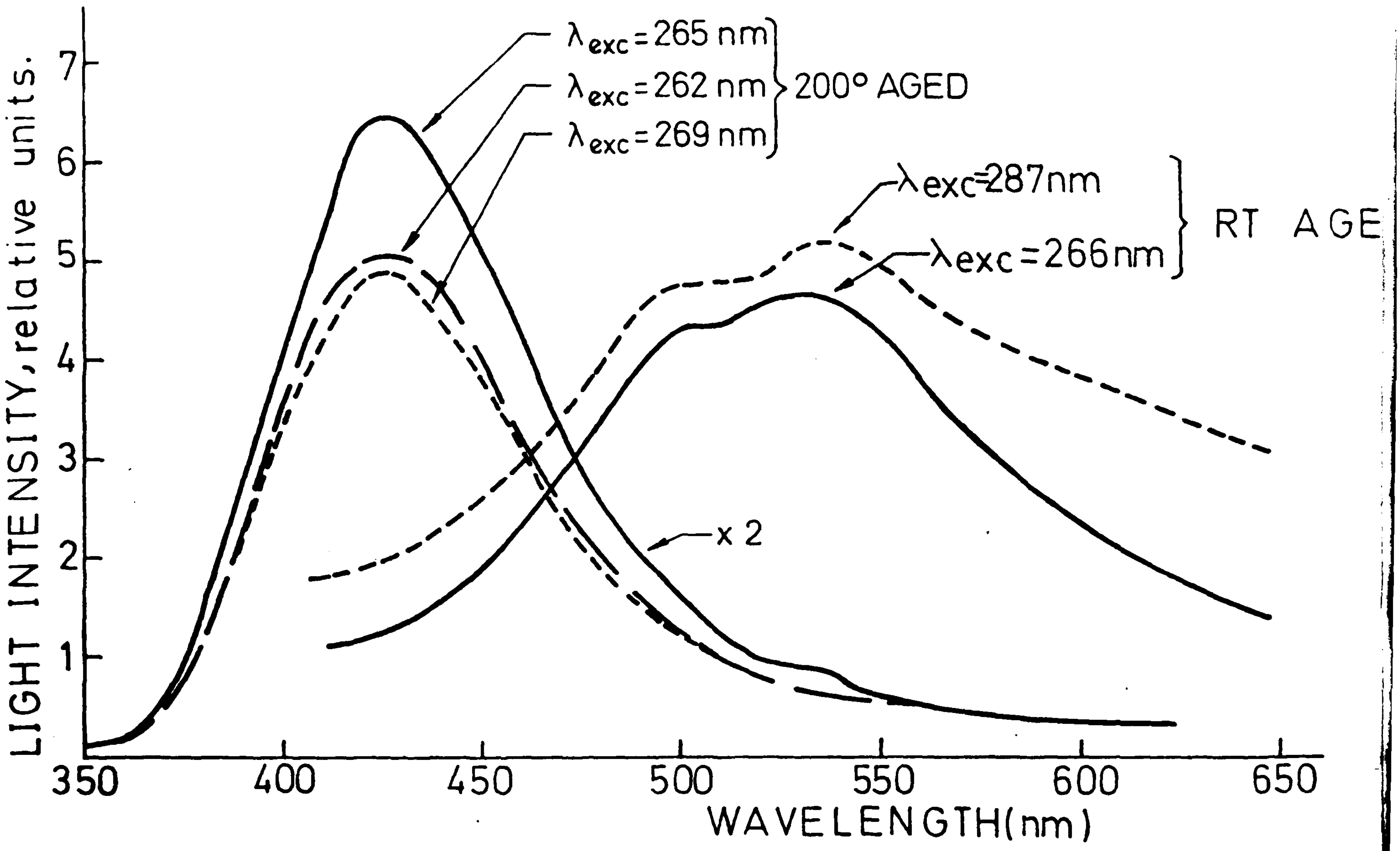
λexc = 265 nm
λexc = 262 nm
λexc = 269 nm
200° AGED
λexc=287nm
λexc = 266nm
RT AGE
x 2
LIGHT INTENSITY, relative units.
1
2
3
4
5
6
7
350
400
450
500
550
600
650
WAVELENGTH(nm)

FIG. 3

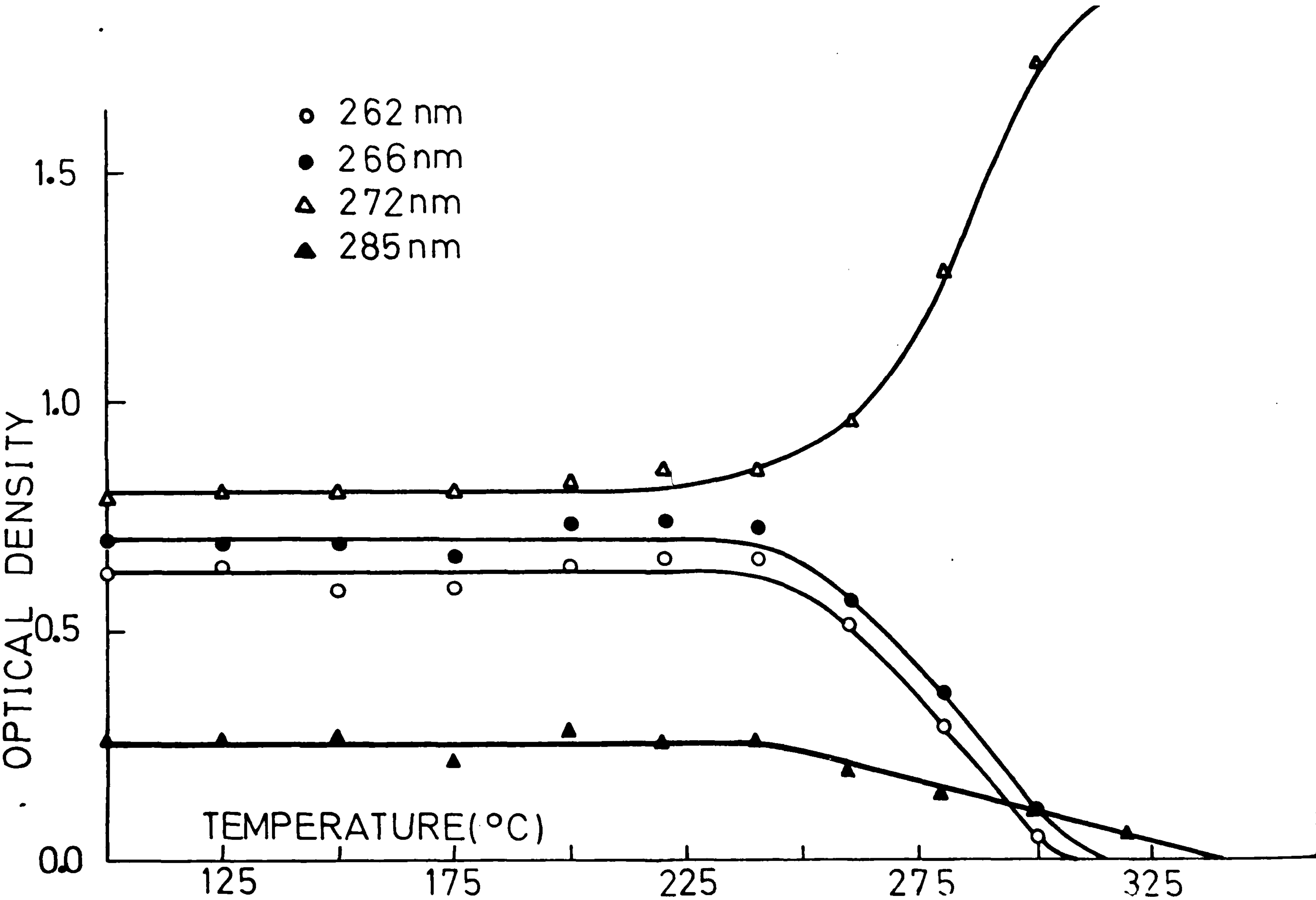

262 nm
266 nm
272 nm
285 nm
OPTICAL DENSITY
1.5
1.0
0.5
0.0
TEMPERATURE(°C)
125
175
225
275
325

FIG. 4

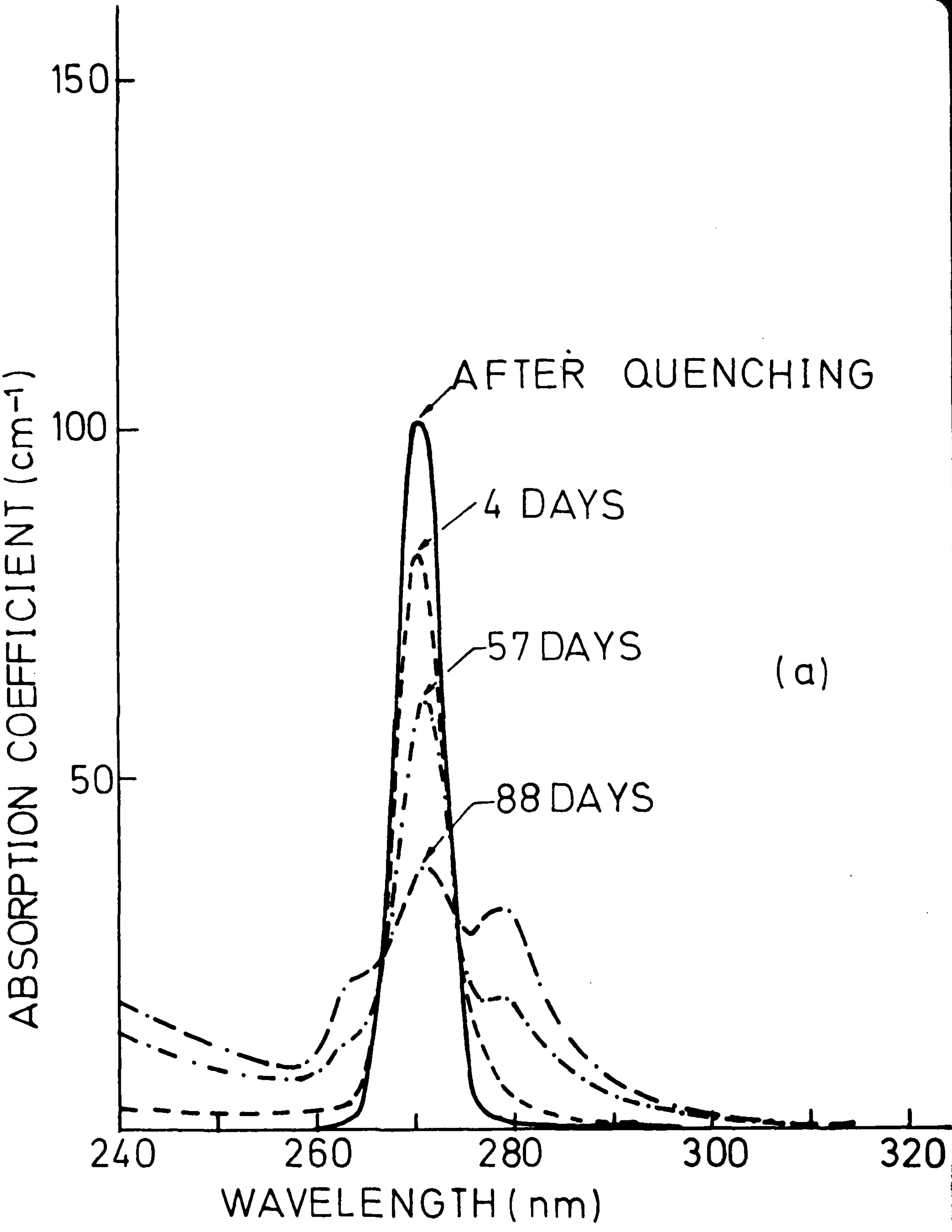

150
100
50
ABSORPTION COEFFICIENT (cm^{-1})
AFTER QUENCHING
4 DAYS
57 DAYS
88 DAYS
(a)
240
260
280
300
320
WAVELENGTH (nm)

FIG. 5

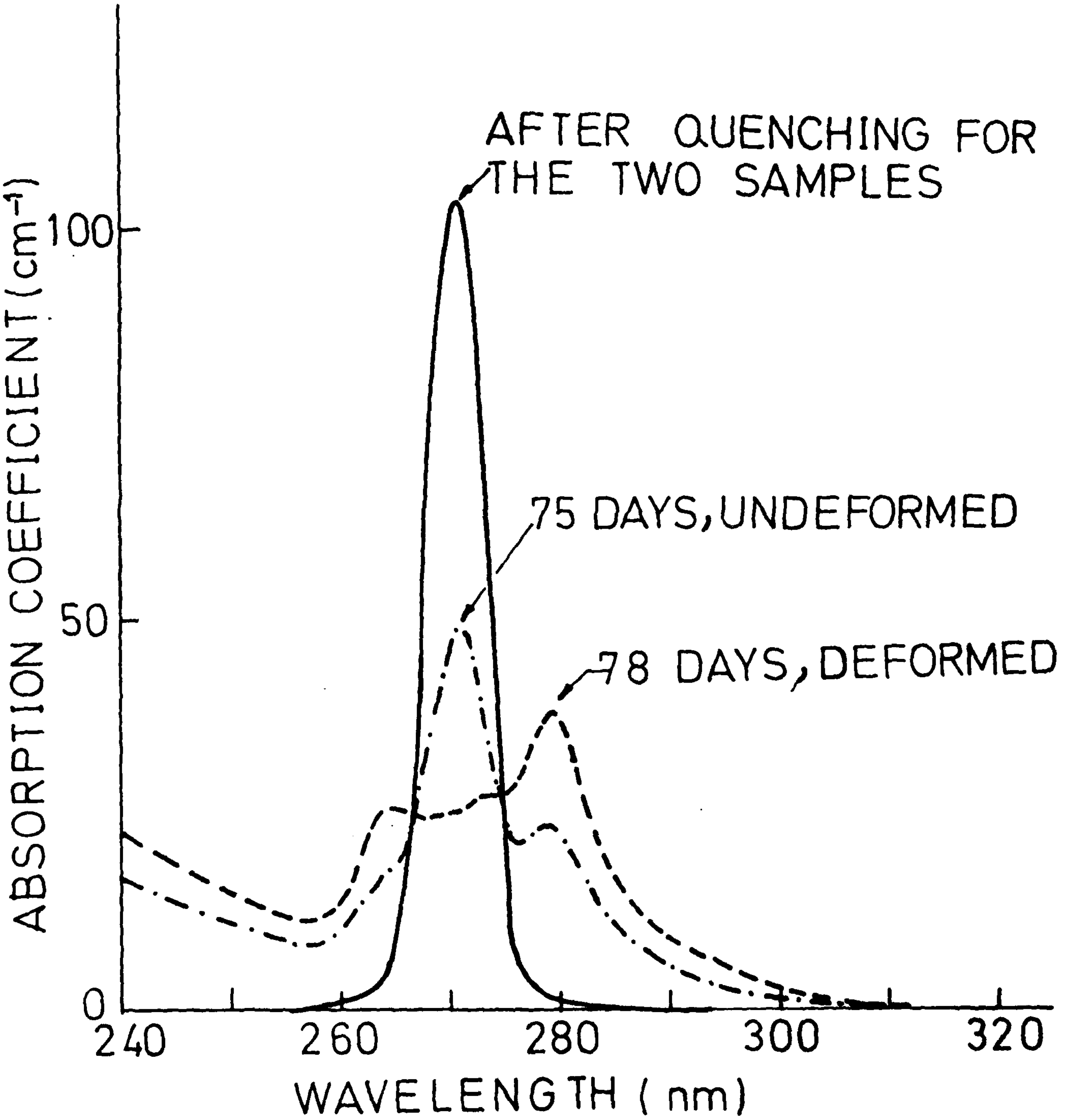
AFTER QUENCHING FOR
THE TWO SAMPLES
75 DAYS, UNDEFORMED
78 DAYS, DEFORMED
ABSORPTION COEFFICIENT (cm^{-1})
100
50
0
240
260
280
300
320
WAVELENGTH (nm)

FIG. 6

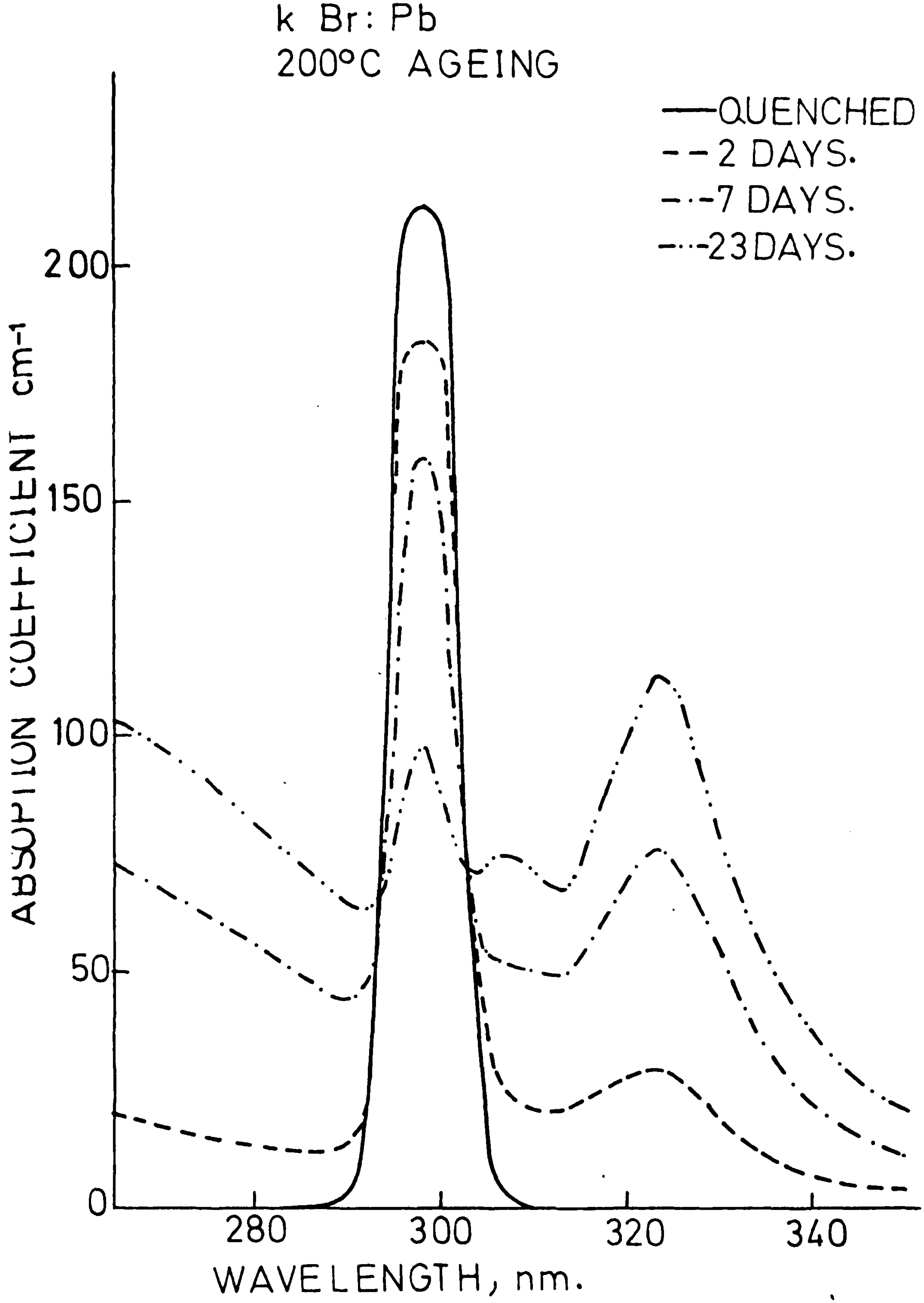
k Br: Pb
200°C AGEING
QUENCHED
2 DAYS.
7 DAYS.
23 DAYS.
ABSORPTION COEFFICIENT cm-1
200
150
100
50
0
280
300
320
340
WAVELENGTH, nm.

FIG. 7

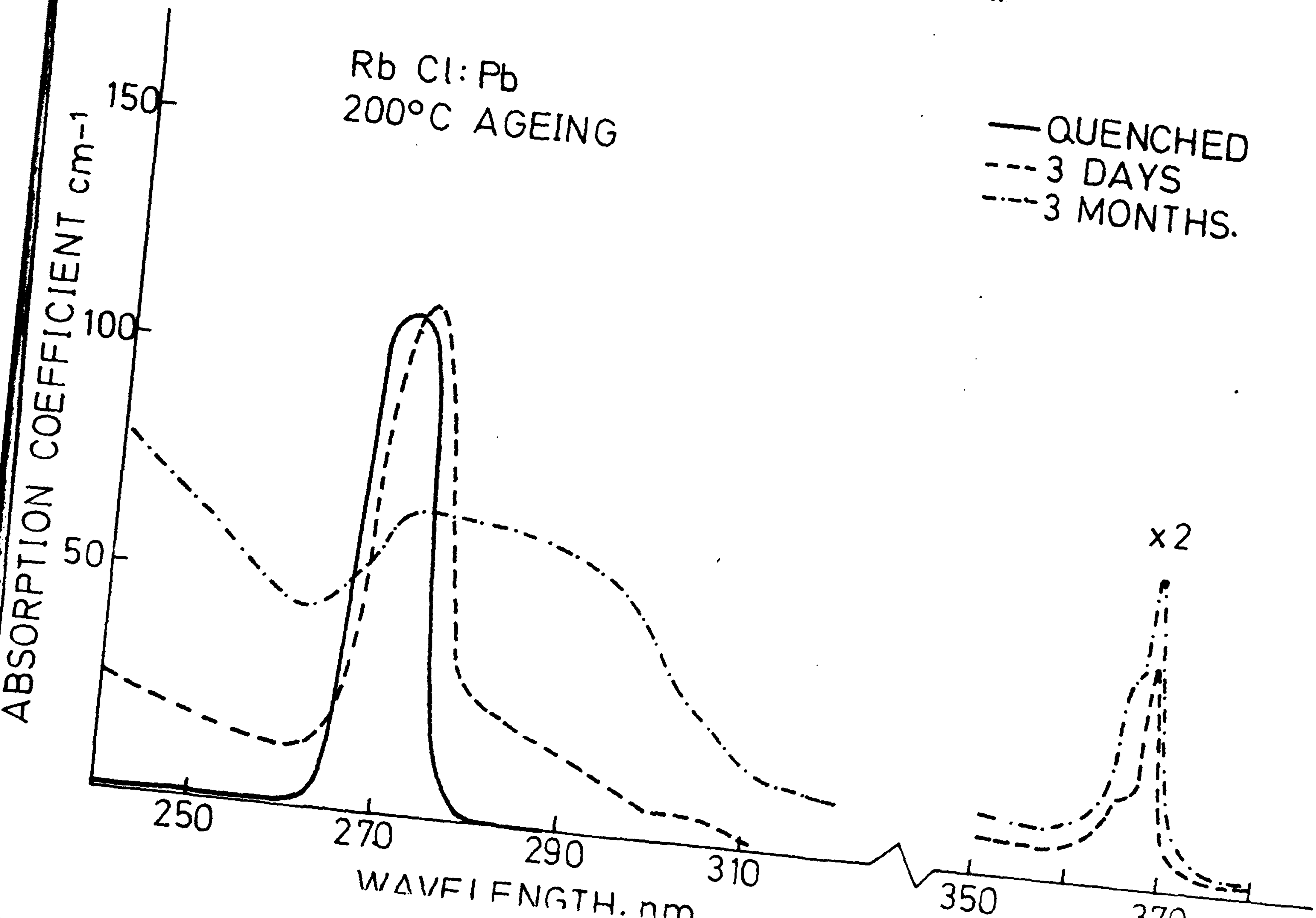
Rb Cl: Pb
200°C AGEING
QUENCHED
3 DAYS
3 MONTHS.
x 2
ABSORPTION COEFFICIENT cm-1
150
100
50
250
270
290
310
350
370
WAVELENGTH. nm.

FIG. 8

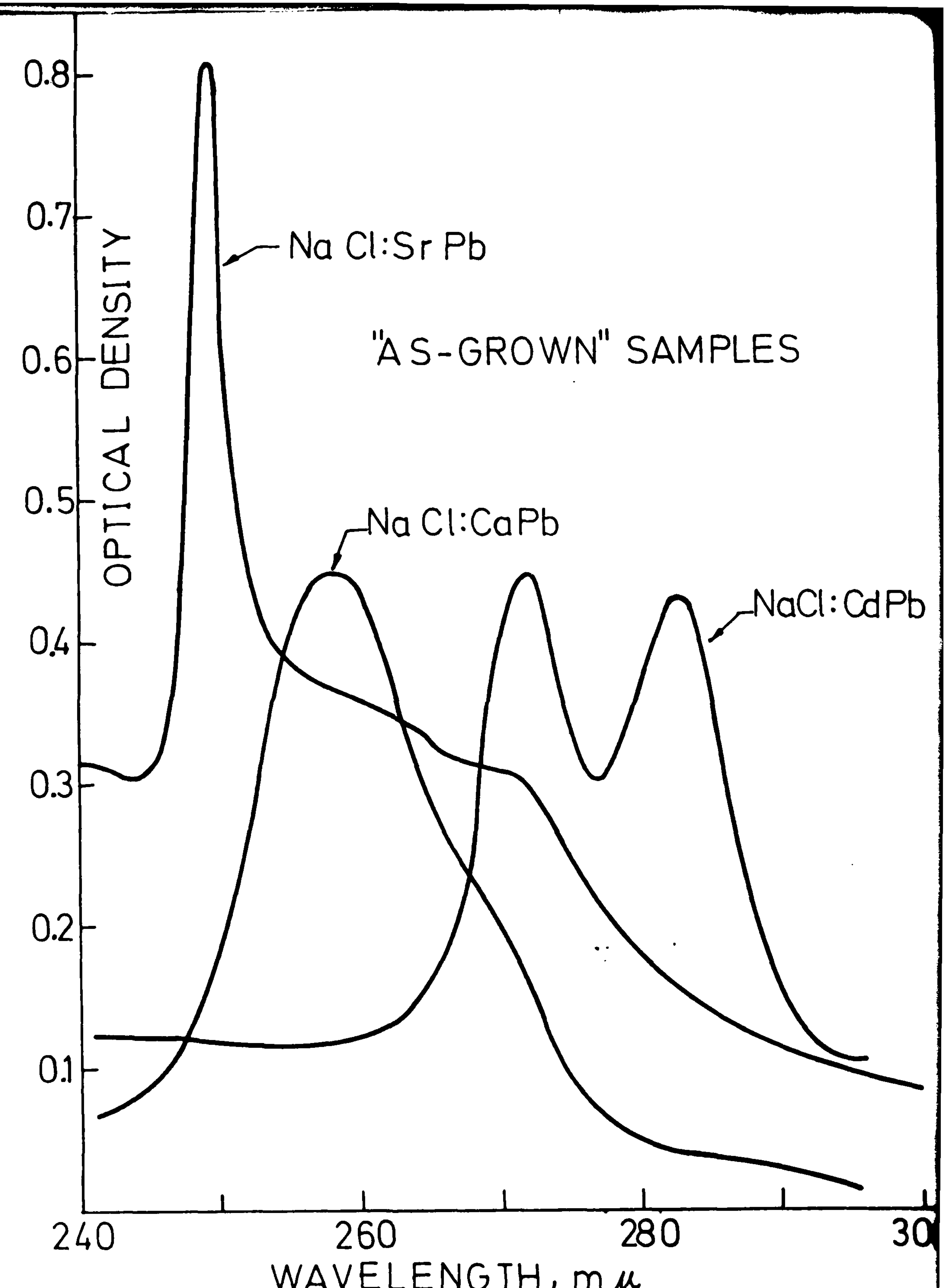
0.8
0.7
0.6
0.5
0.4
0.3
0.2
0.1
OPTICAL DENSITY
Na Cl:Sr Pb
"A S-GROWN" SAMPLES
Na Cl:CaPb
NaCl:CdPb
240
260
280
30
WAVELENGTH, mμ

FIG. 9

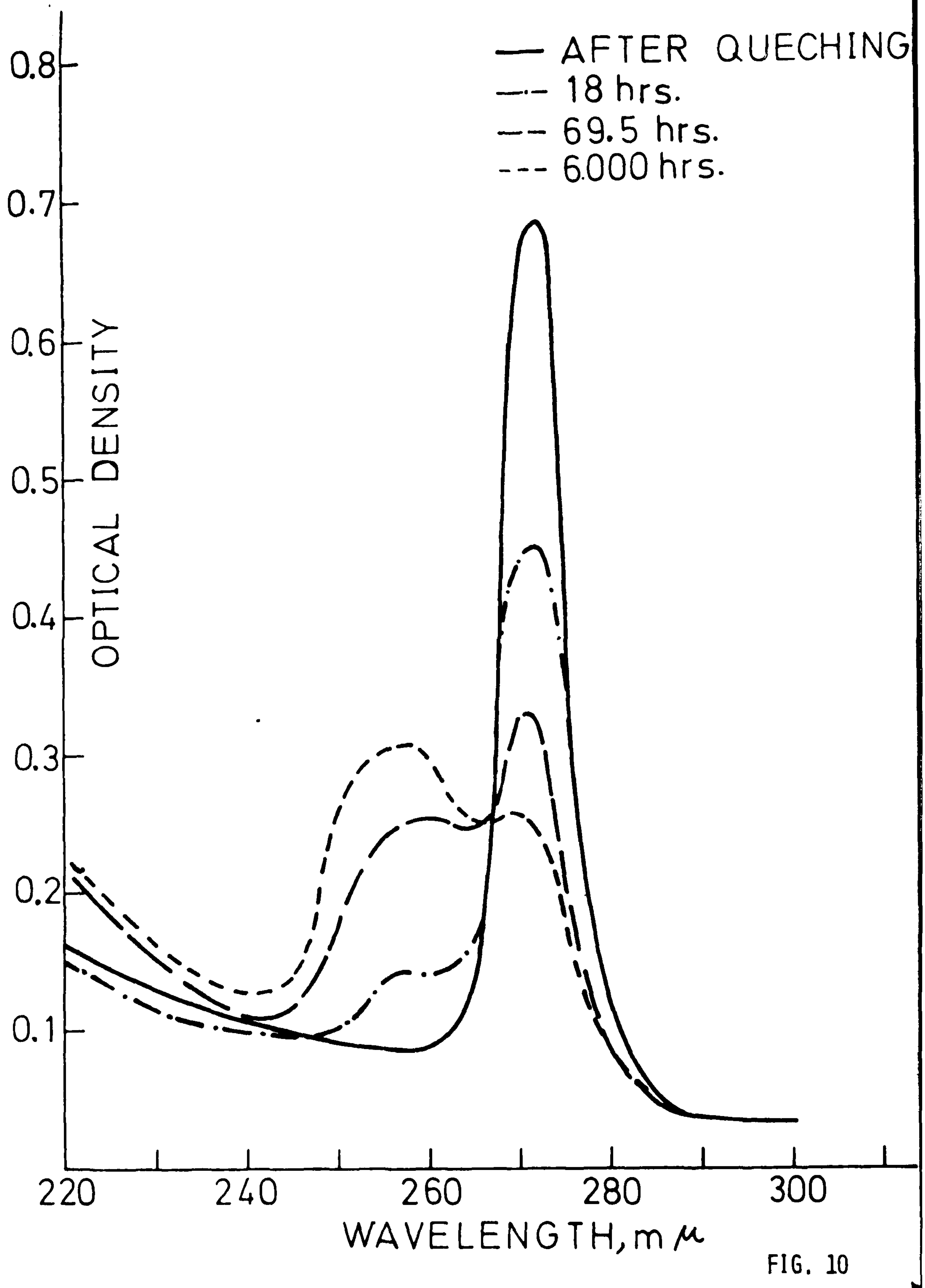

AFTER QUECHING
18 hrs.
69.5 hrs.
6.000 hrs.
0.8
0.7
0.6
0.5
0.4
0.3
0.2
0.1
OPTICAL DENSITY
220
240
260
280
300
WAVELENGTH, m μ

FIG. 10

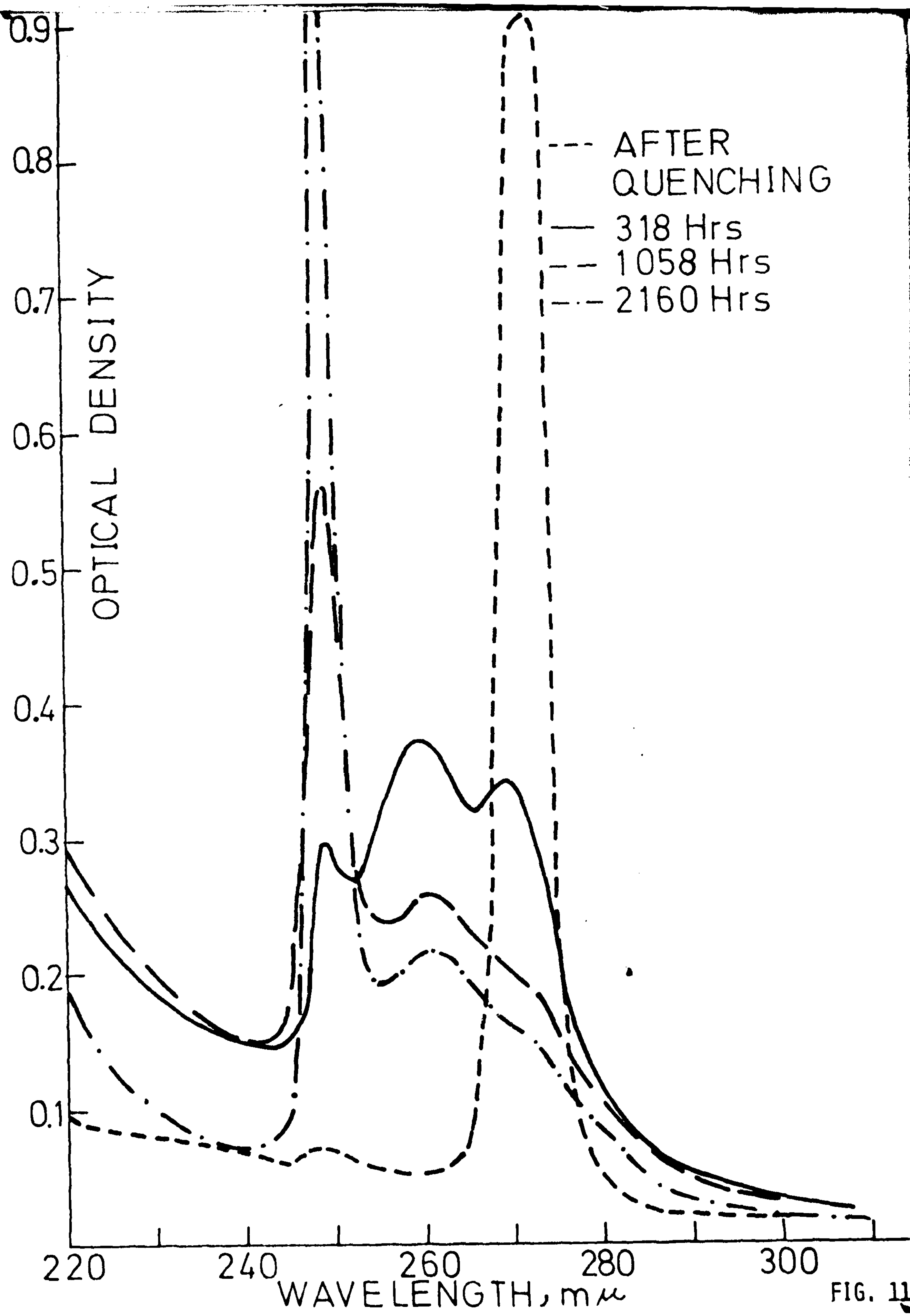

0.9
0.8
0.7
0.6
0.5
0.4
0.3
0.2
0.1
OPTICAL DENSITY
AFTER QUENCHING
318 Hrs
1058 Hrs
2160 Hrs
220
240
260
280
300
WAVELENGTH, mμ

FIG. 11

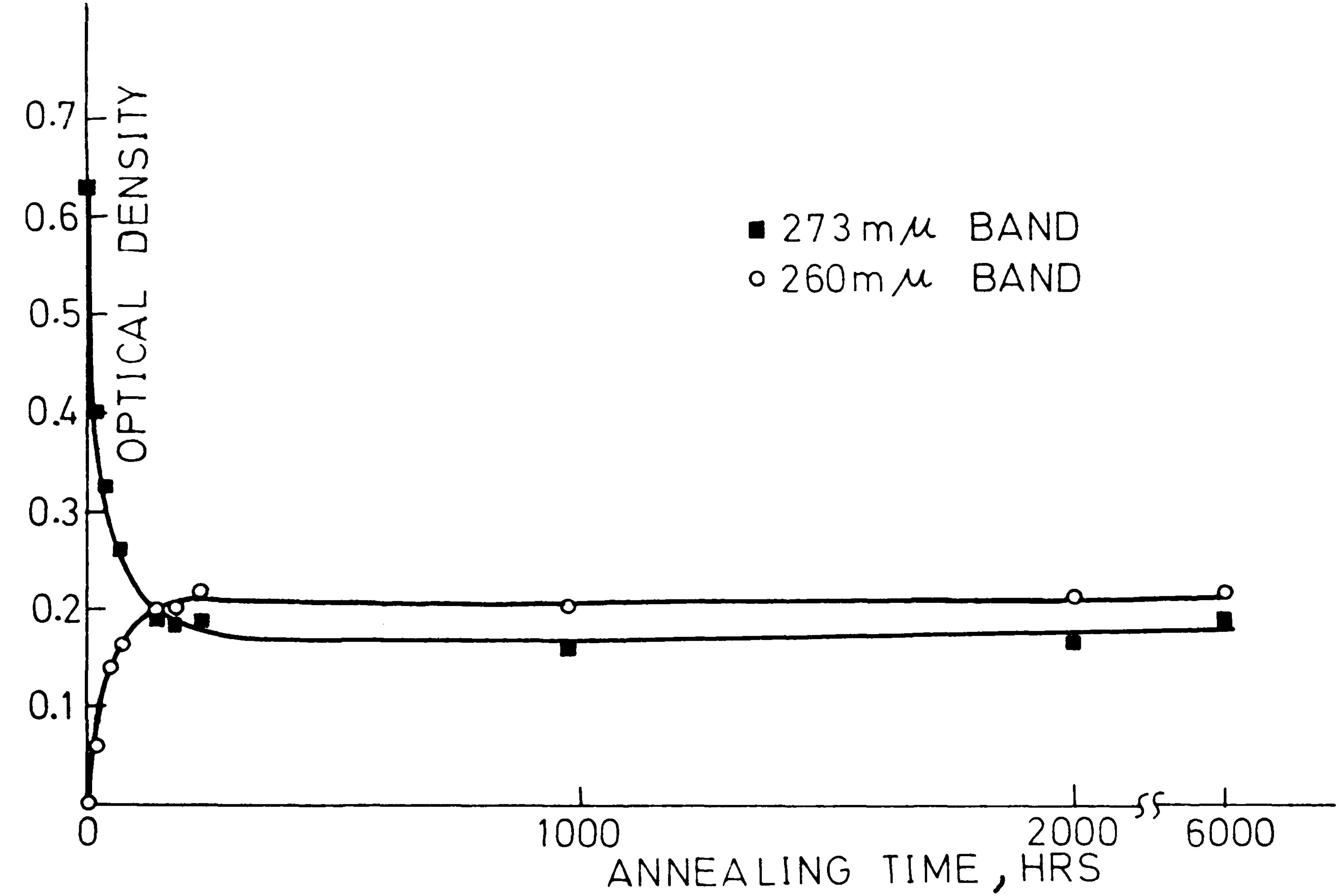

0.7
0.6
0.5
0.4
0.3
0.2
0.1
OPTICAL DENSITY
■ 273 mμ BAND
○ 260 mμ BAND
0
1000
2000
6000
ANNEALING TIME, HRS

FIG. 12

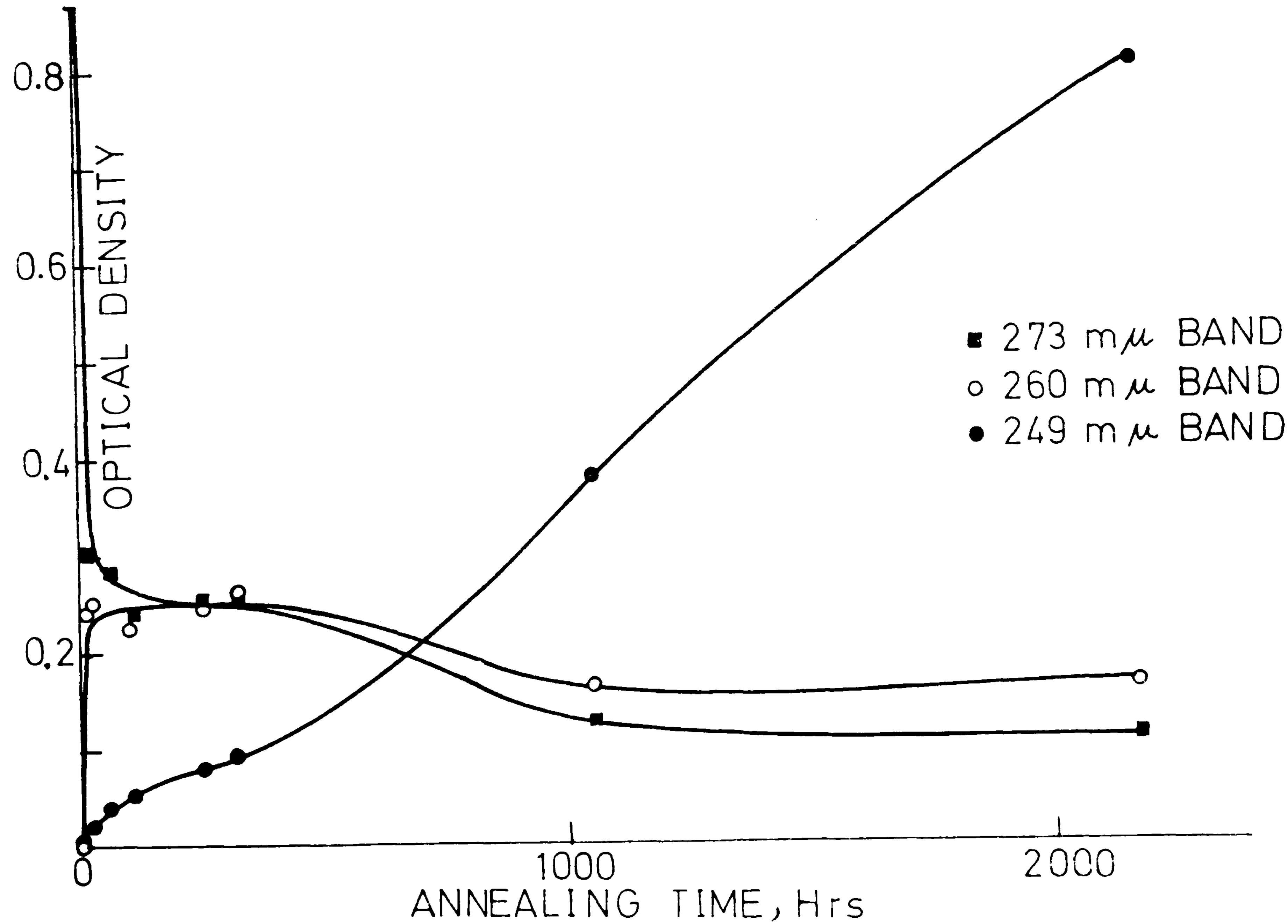

0.8
0.6
0.4
0.2
0
1000
2000
OPTICAL DENSITY
ANNEALING TIME, Hrs
273 mμ BAND
260 mμ BAND
249 mμ BAND

FIG. 13

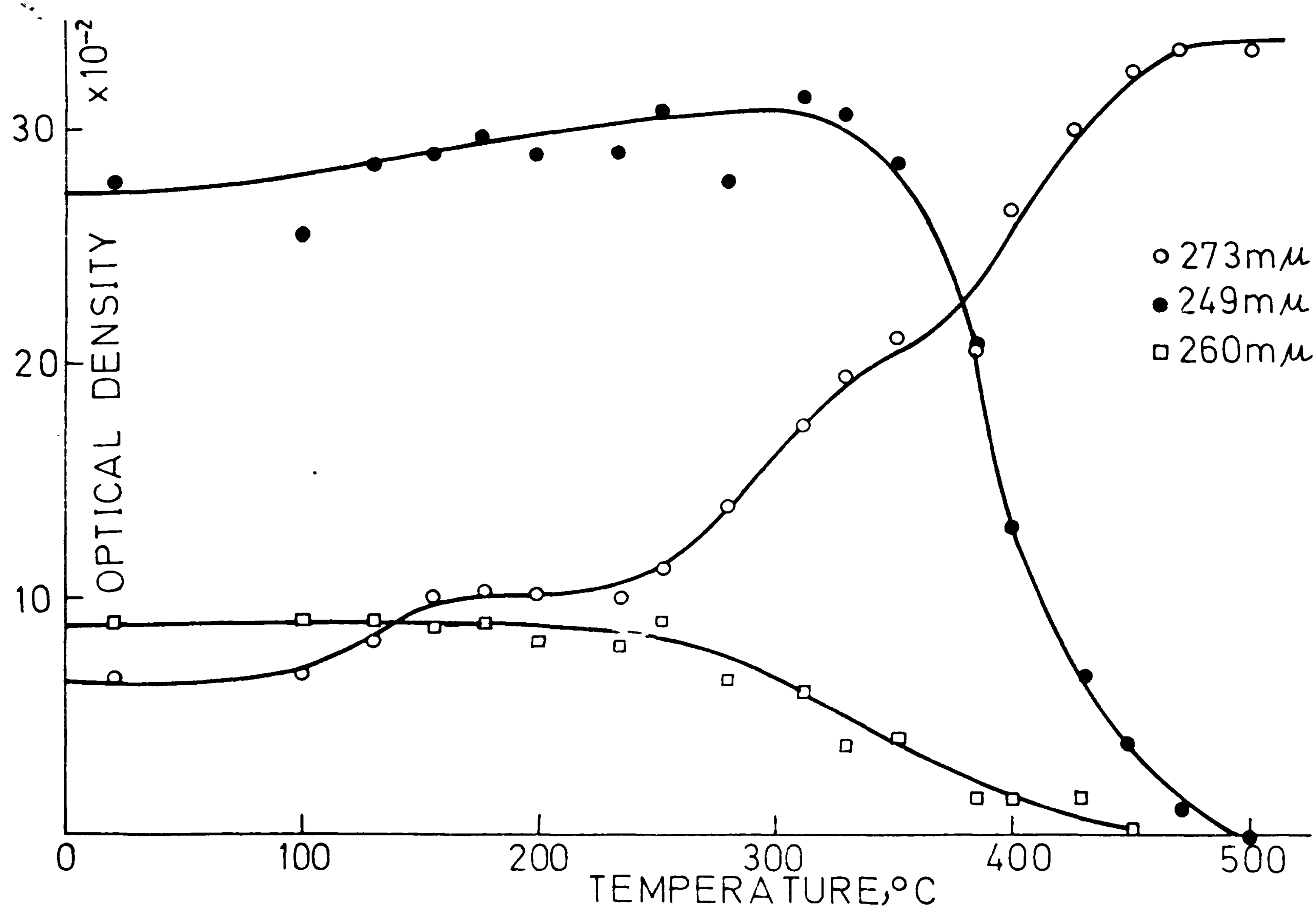

OPTICAL DENSITY
x10⁻²
30
20
10
0
100
200
300
400
500
TEMPERATURE, °C
○ 273mμ
● 249mμ
□ 260mμ

FIG. 14

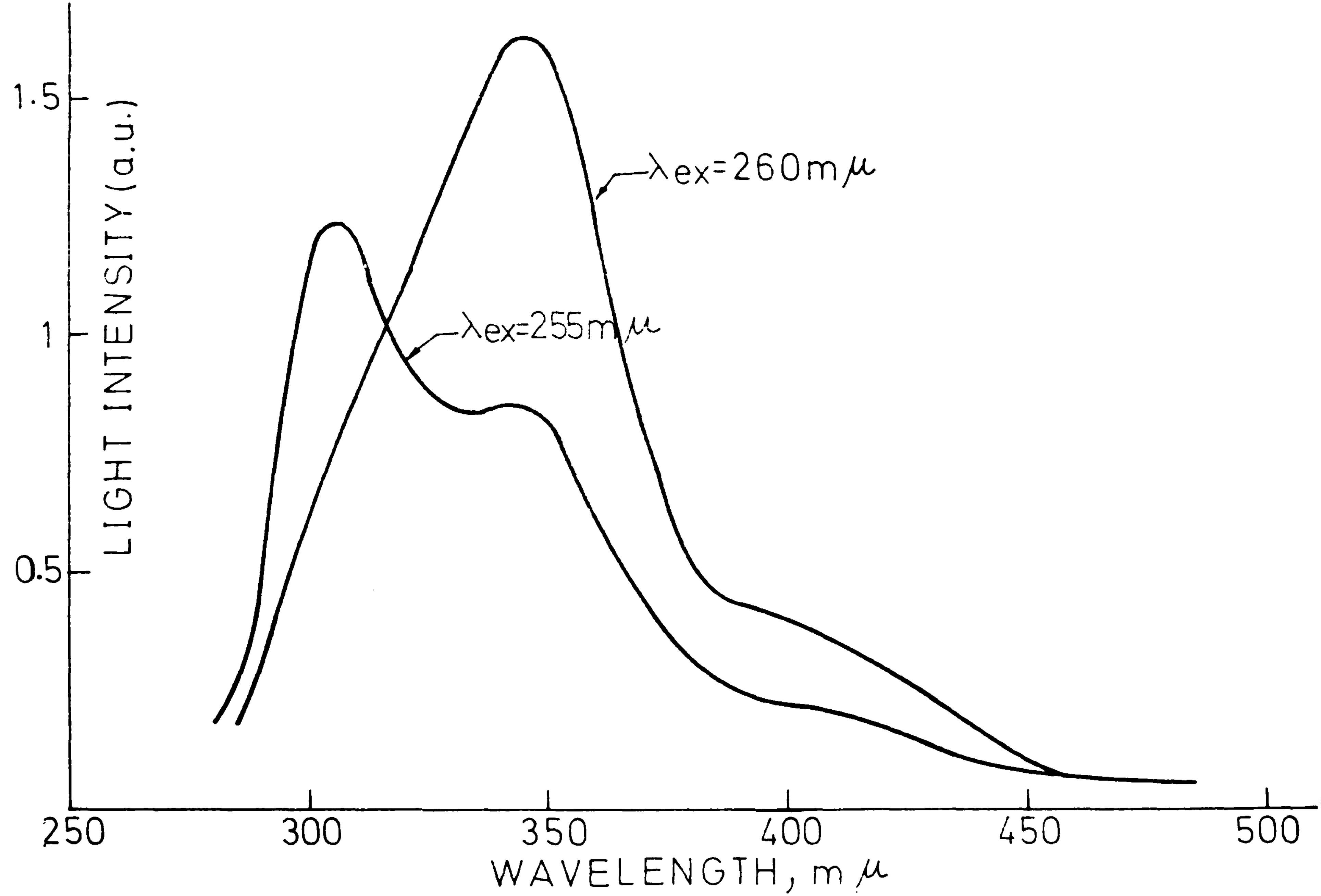

1.5
1
0.5
LIGHT INTENSITY (a.u.)
λex=260mμ
λex=255mμ
250
300
350
400
450
500
WAVELENGTH, mμ

FIG. 15

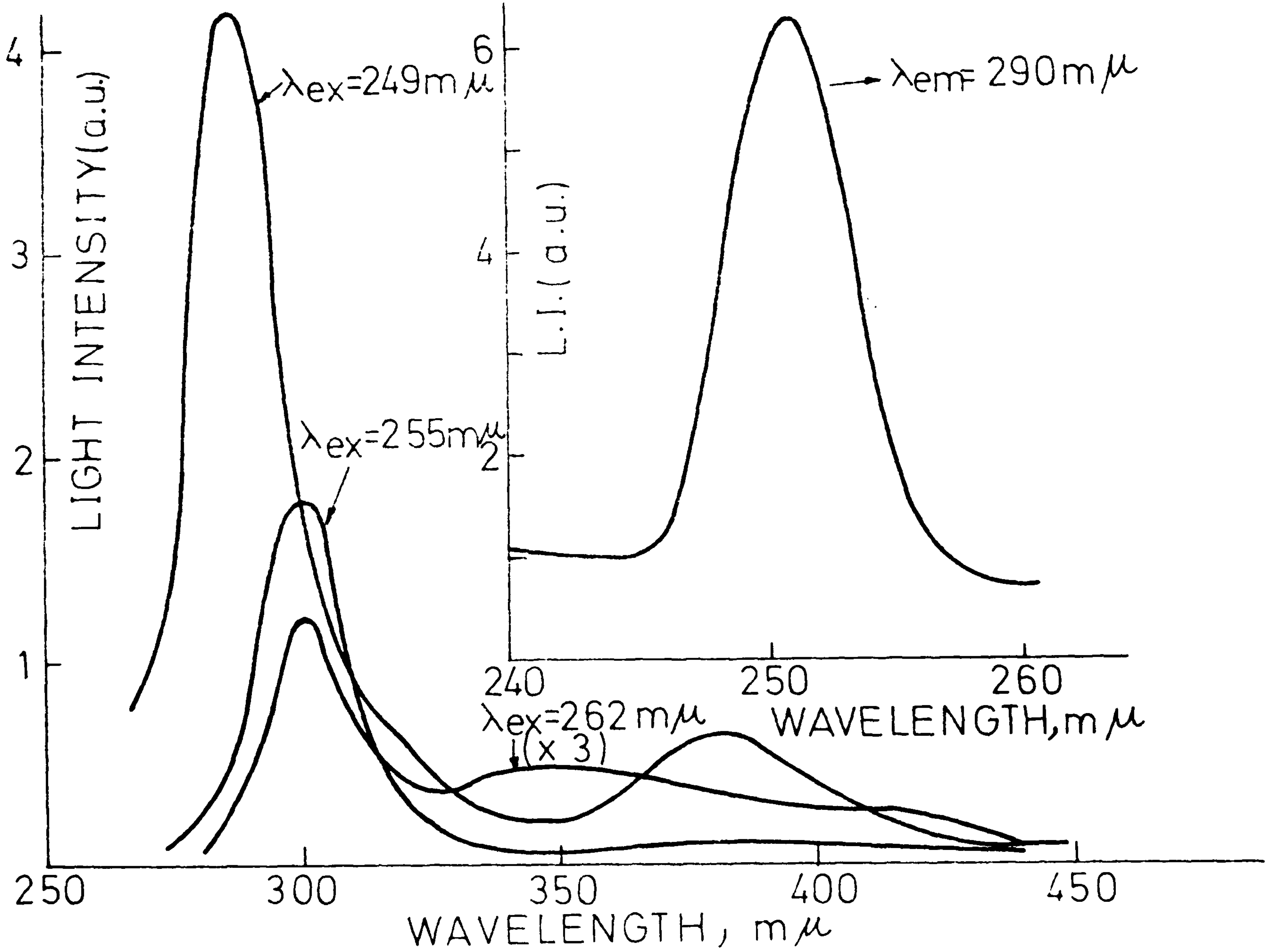

LIGHT INTENSITY(a.u.)
4
3
2
1
250
300
350
400
450
WAVELENGTH, mμ
λex=249mμ
λex=255mμ
λex=262mμ
(x 3)
L.I.(a.u.)
6
4
2
240
250
260
WAVELENGTH, mμ
λem= 290mμ

FIG. 16

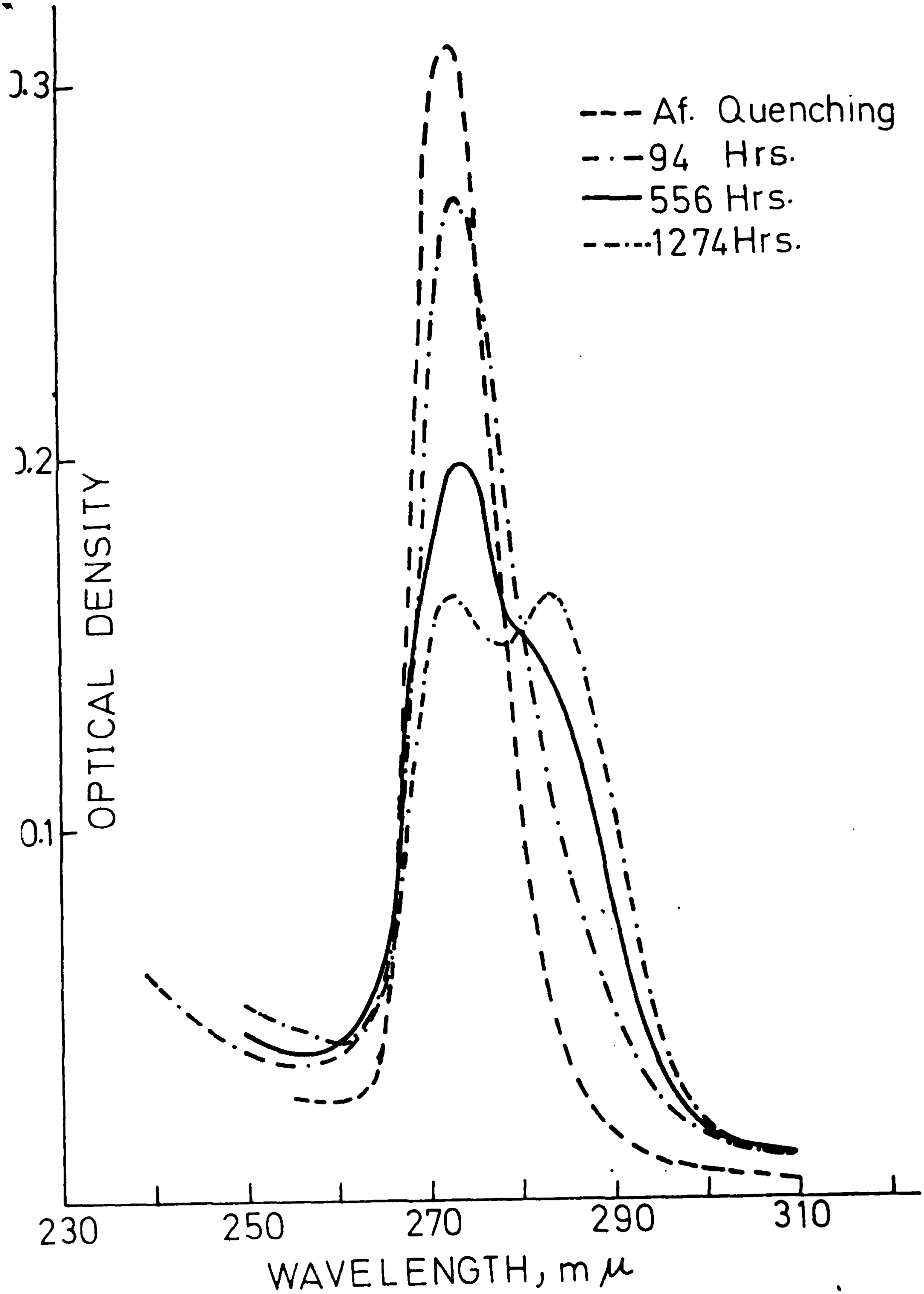
0.3
0.2
0.1
OPTICAL DENSITY
Af. Quenching
94 Hrs.
556 Hrs.
1274 Hrs.
230
250
270
290
310
WAVELENGTH, mμ

FIG. 17

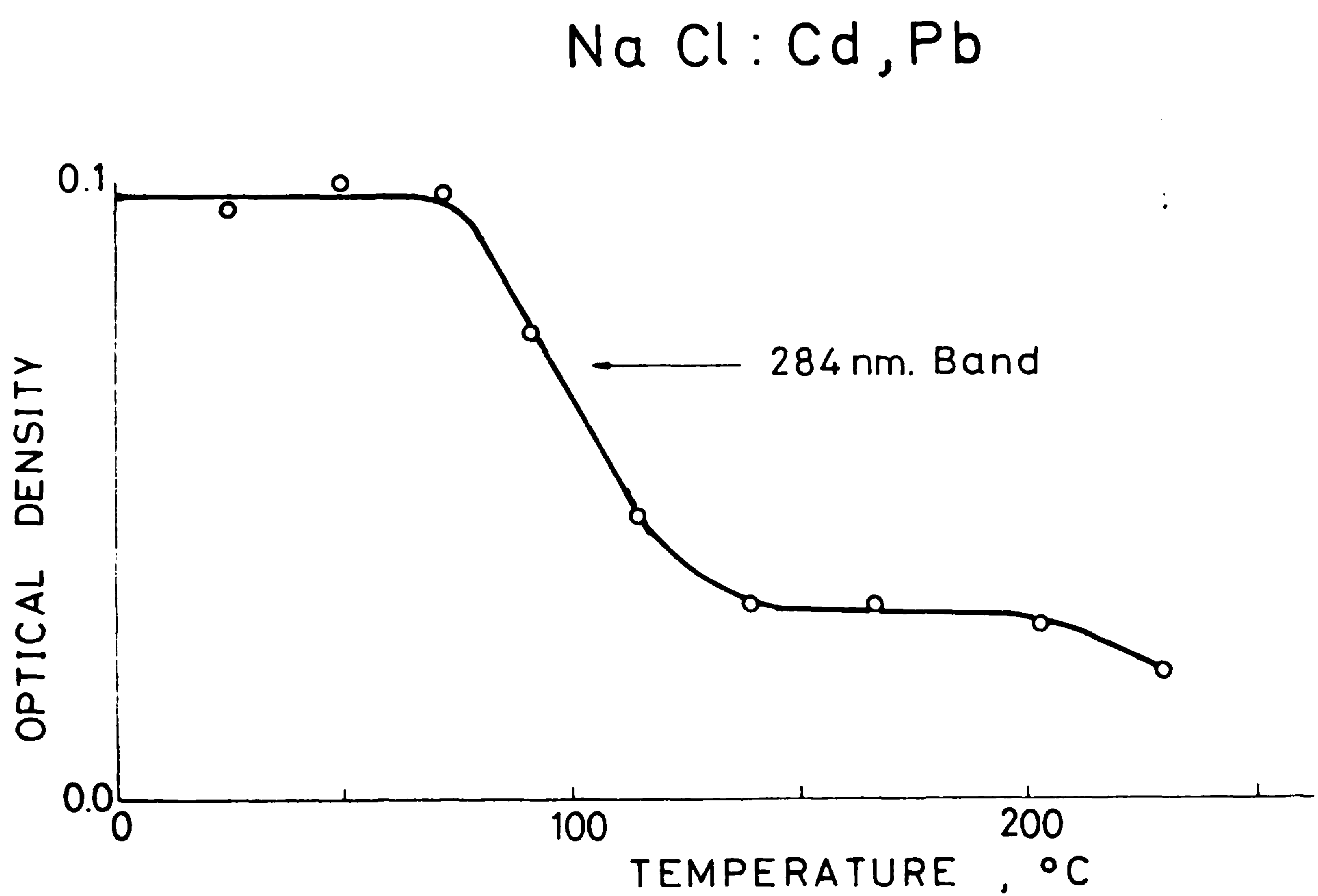
Na Cl : Cd , Pb
0.1
0.0
OPTICAL DENSITY
284 nm. Band
0
100
200
TEMPERATURE , °C

FIG. 18

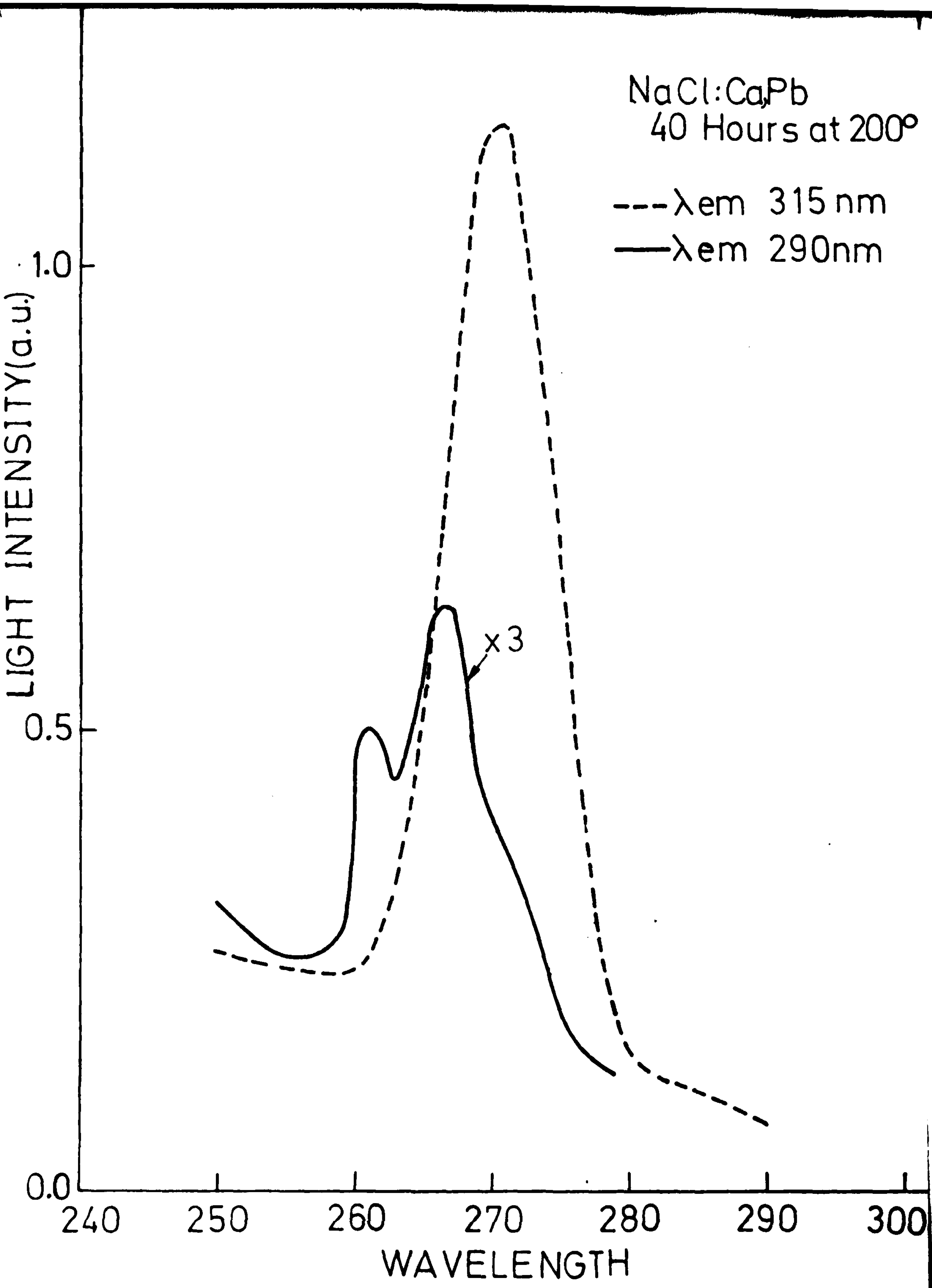
NaCl:Ca,Pb
40 Hours at 200°
---λem 315 nm
—λem 290nm
LIGHT INTENSITY(a.u.)
1.0
0.5
0.0
x3
240
250
260
270
280
290
300
WAVELENGTH

FIG. 19

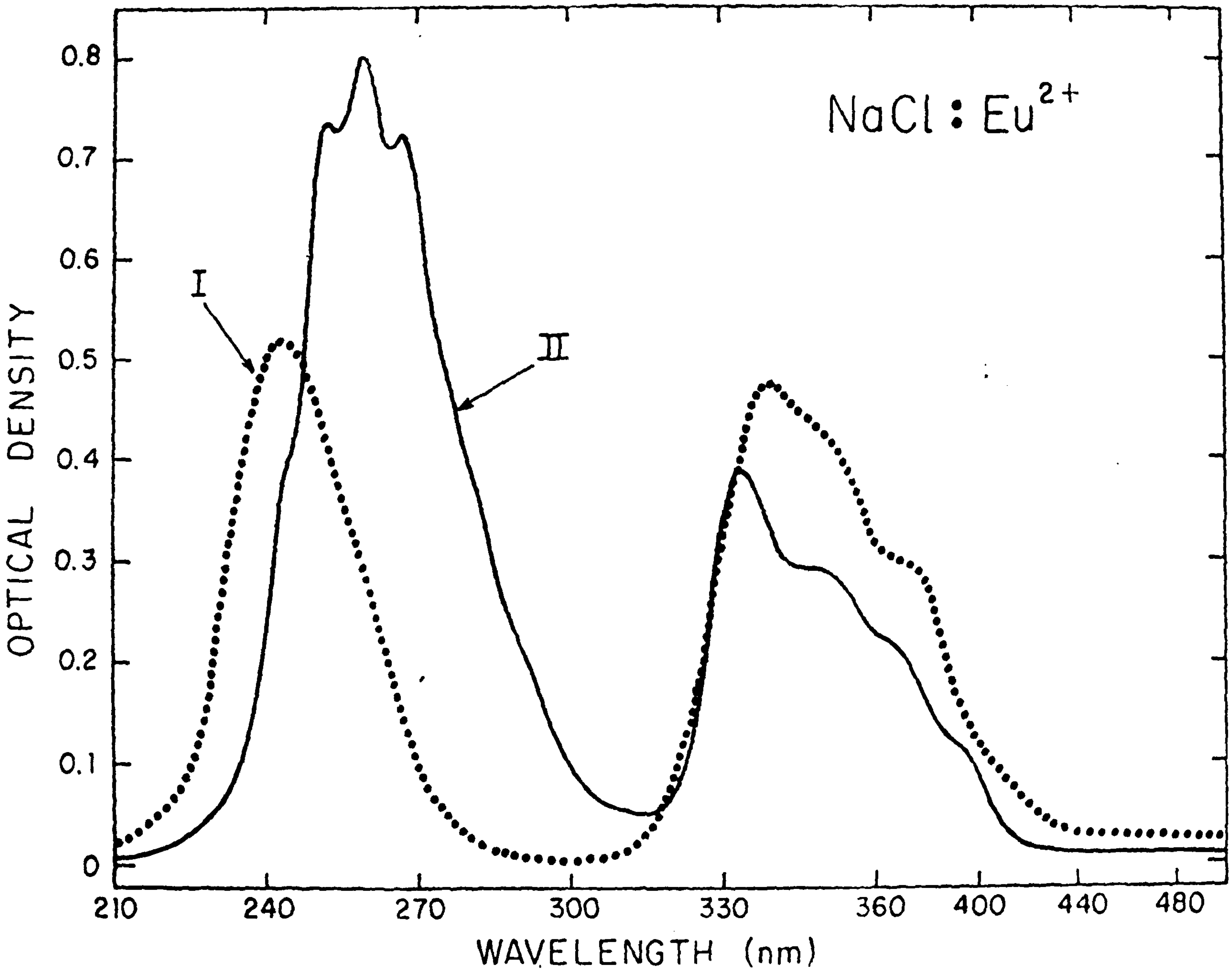
NaCl : Eu^{2+}
I
II
OPTICAL DENSITY
0.8
0.7
0.6
0.5
0.4
0.3
0.2
0.1
0
210
240
270
300
330
360
400
440
480
WAVELENGTH (nm)

FIG. 20

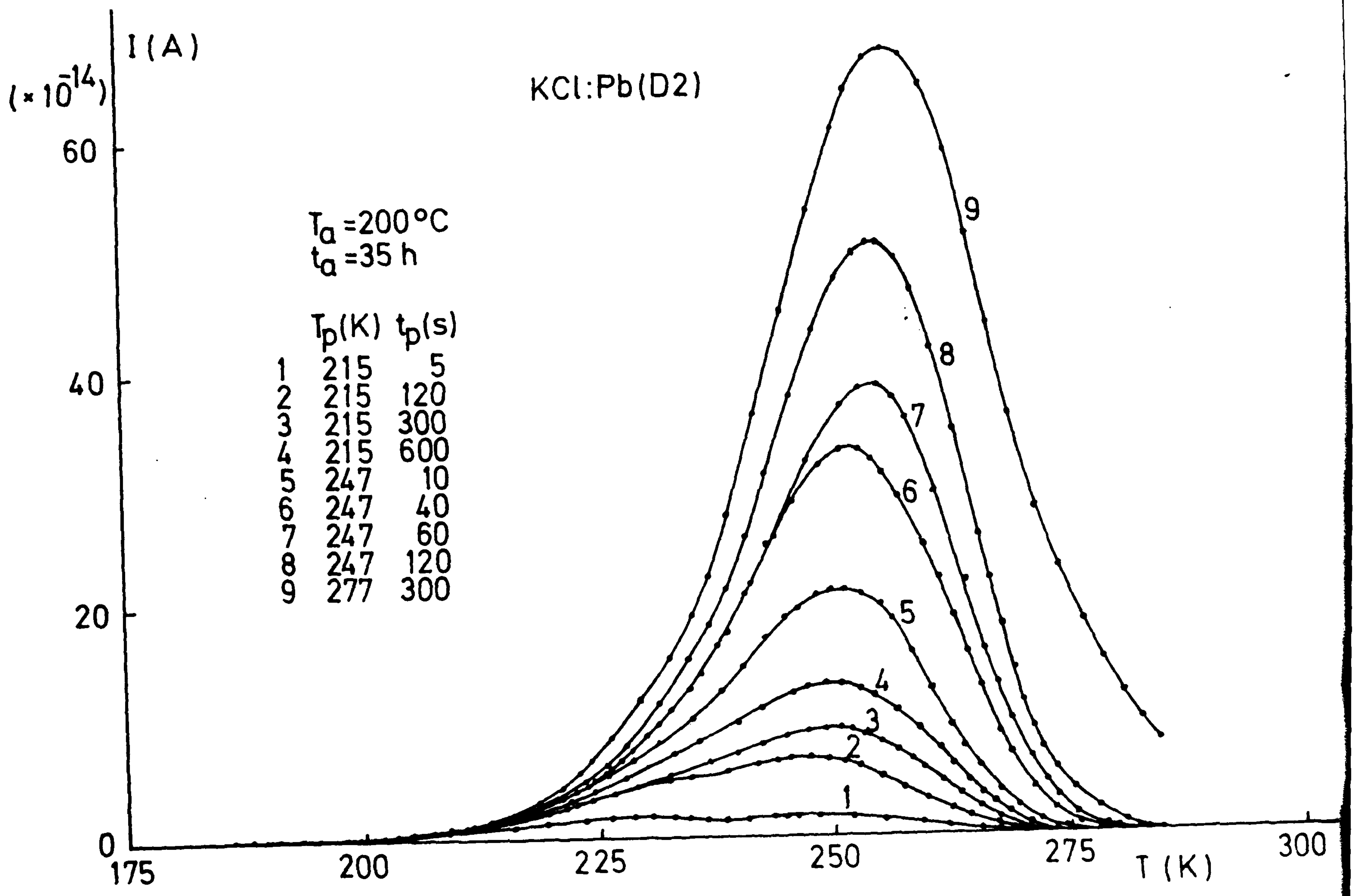

I (A)
(×10^{-14})
KCl:Pb(D2)
T_a =200°C
t_a =35 h
T_p(K) t_p(s)
1 215 5
2 215 120
3 215 300
4 215 600
5 247 10
6 247 40
7 247 60
8 247 120
9 277 300
0
20
40
60
175
200
225
250
275
300
T (K)
1
2
3
4
5
6
7
8
9

FIG. 21

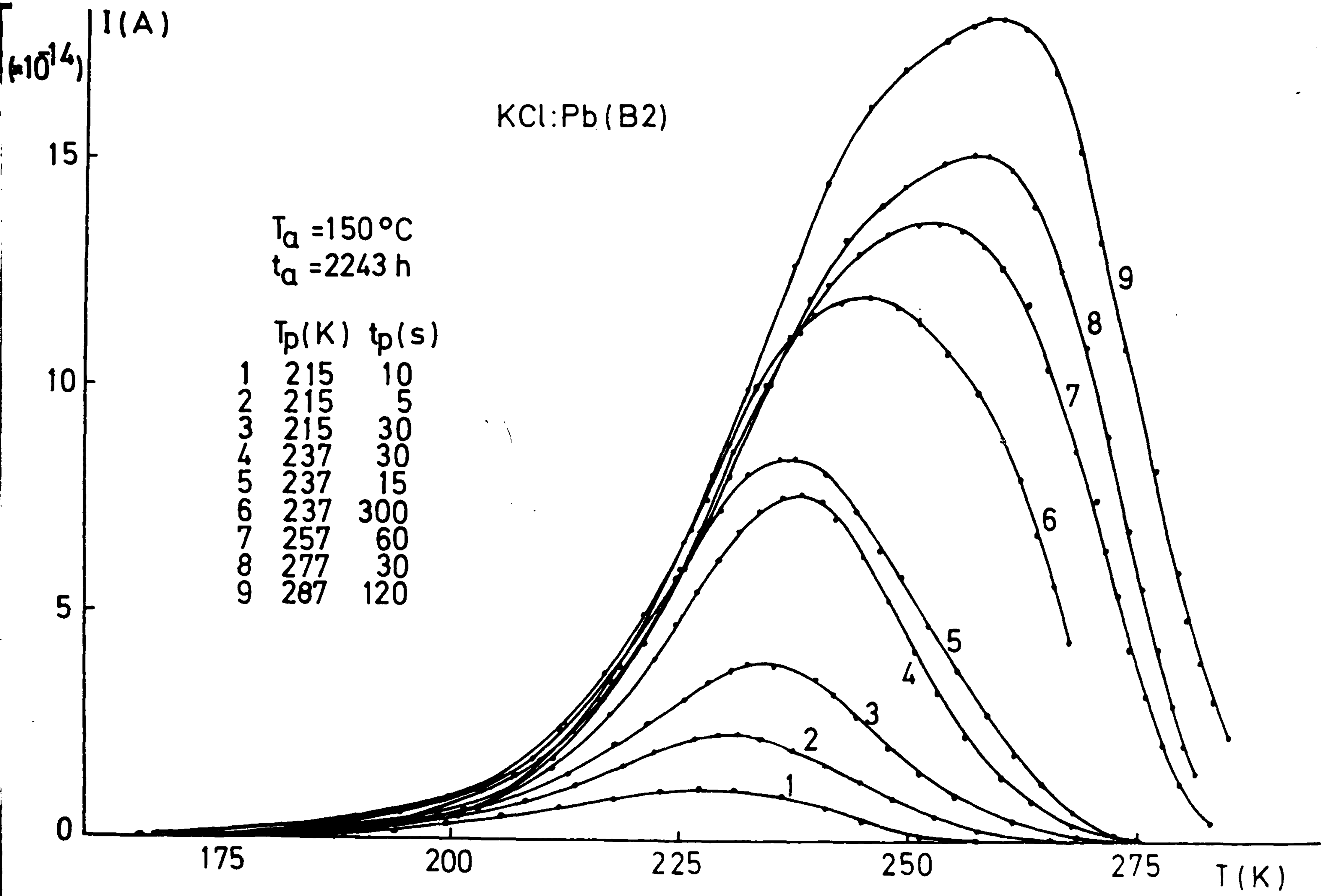
I(A)
(×10⁻¹⁴)
KCl:Pb(B2)
T_a =150°C
t_a =2243 h
T_p(K) t_p(s)
1 215 10
2 215 5
3 215 30
4 237 30
5 237 15
6 237 300
7 257 60
8 277 30
9 287 120
15
10
5
0
175
200
225
250
275
T(K)
1
2
3
4
5
6
7
8
9

FIG. 22

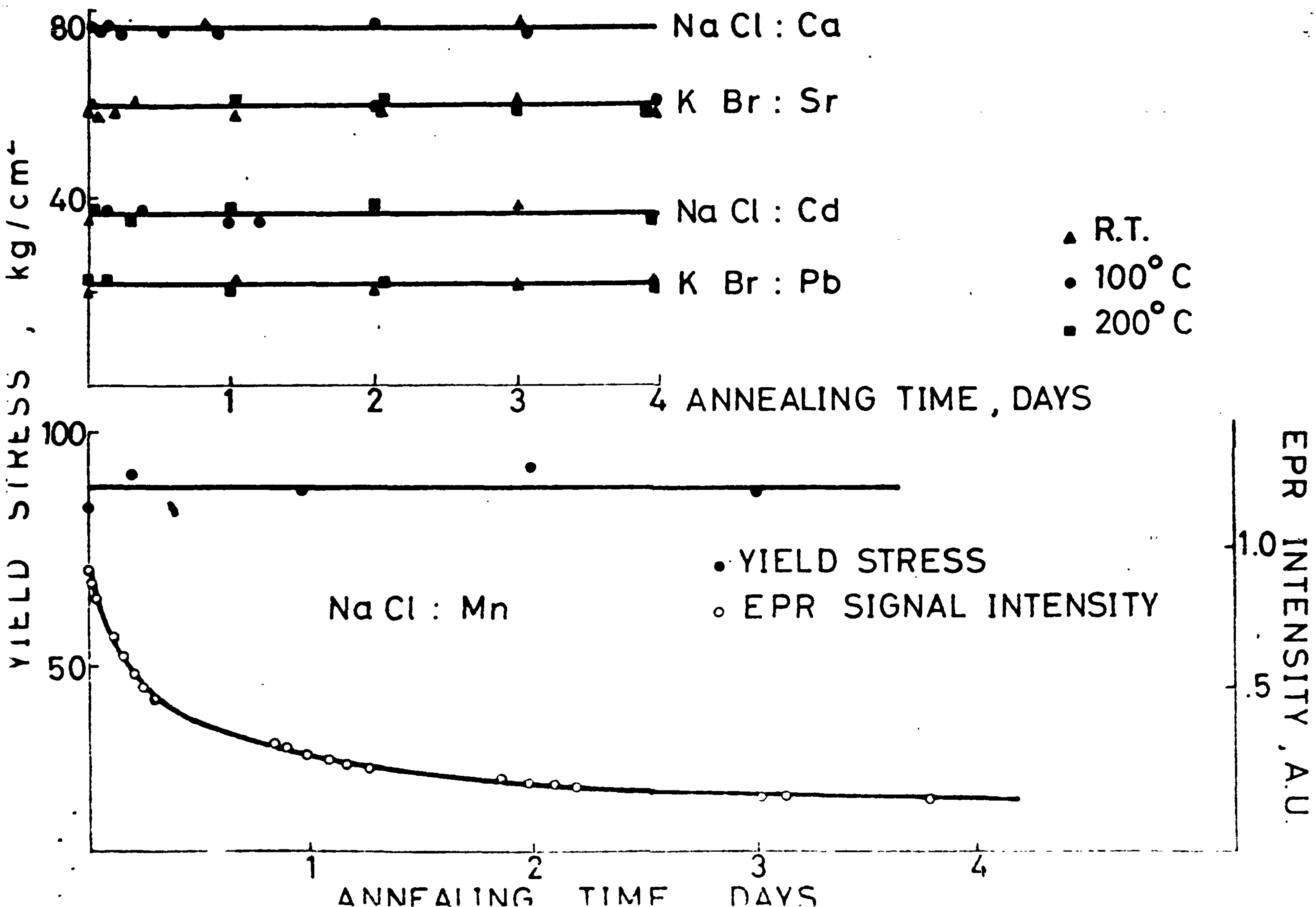

80
40
100
50
YIELD STRESS, kg/cm²
Na Cl : Ca
K Br : Sr
Na Cl : Cd
K Br : Pb
R.T.
100° C
200° C
1
2
3
4
ANNEALING TIME, DAYS
Na Cl : Mn
YIELD STRESS
EPR SIGNAL INTENSITY
1.0
.5
EPR INTENSITY, A.U.
ANNEALING TIME DAYS

FIG. 23

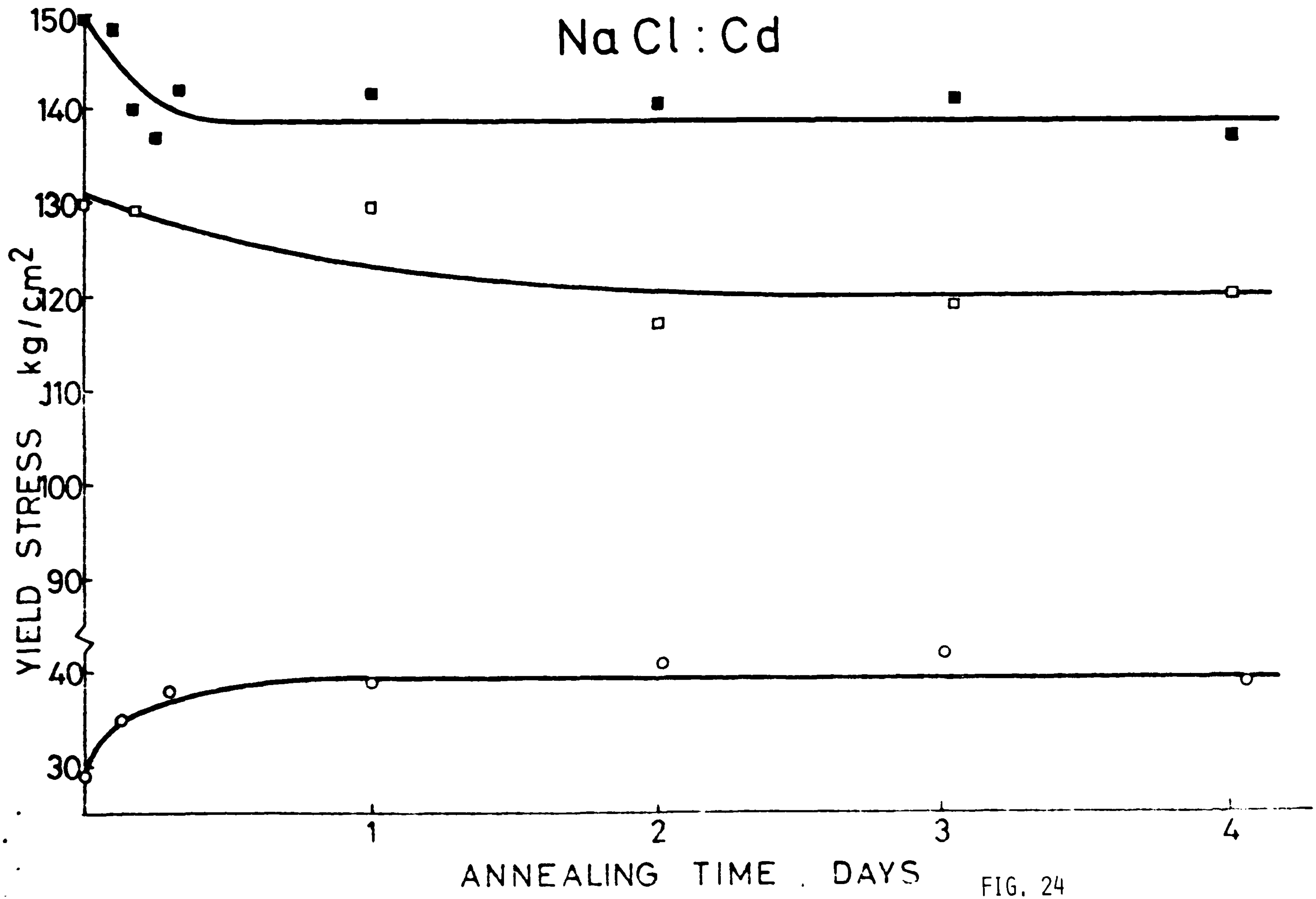
NaCl : Cd
YIELD STRESS kg/cm²
150
140
130
120
110
100
90
40
30
1
2
3
4
ANNEALING TIME . DAYS

FIG. 24

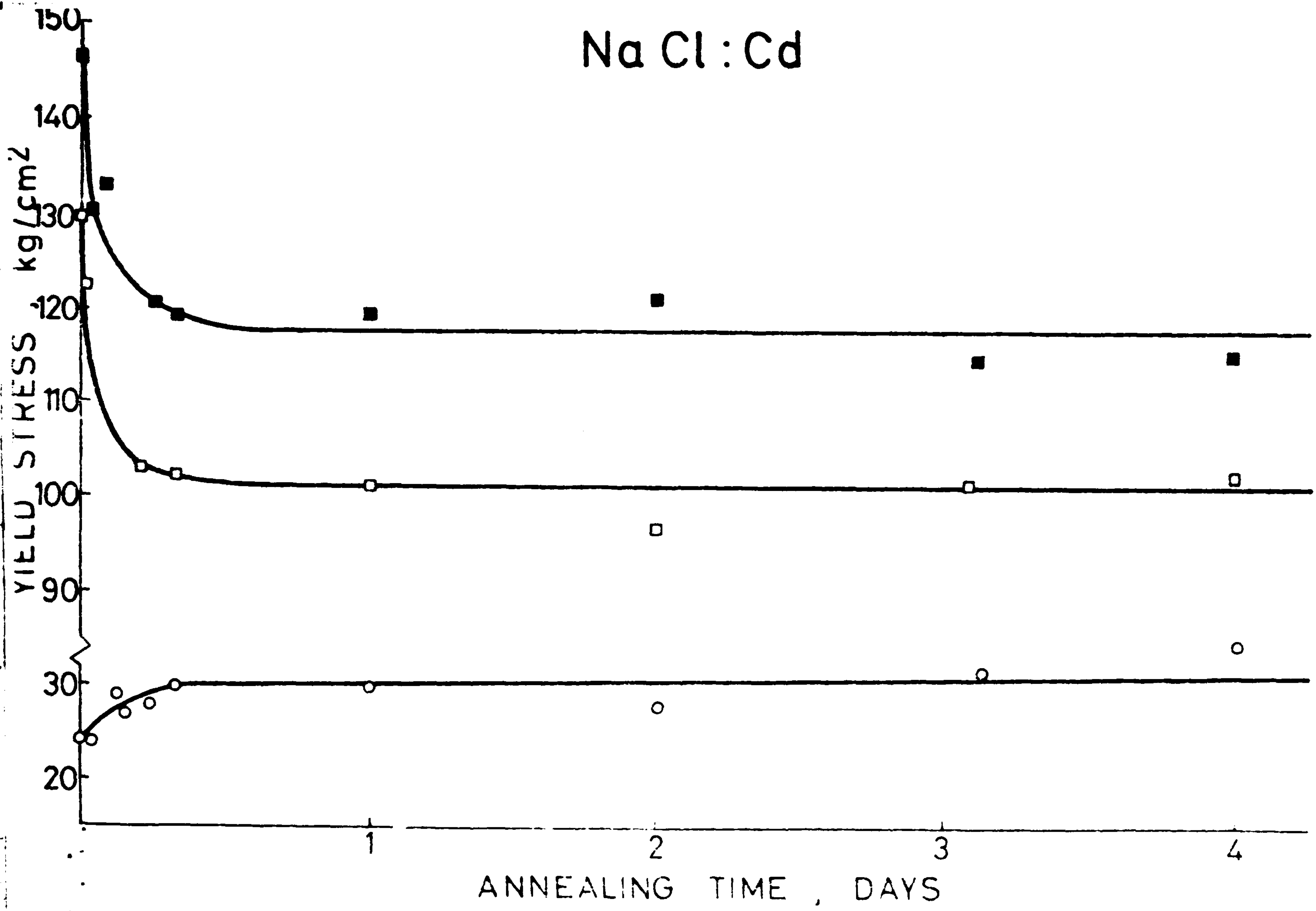

Na Cl : Cd
YIELD STRESS kg/cm²
150
140
130
120
110
100
90
30
20
1
2
3
4
ANNEALING TIME , DAYS

FIG. 25

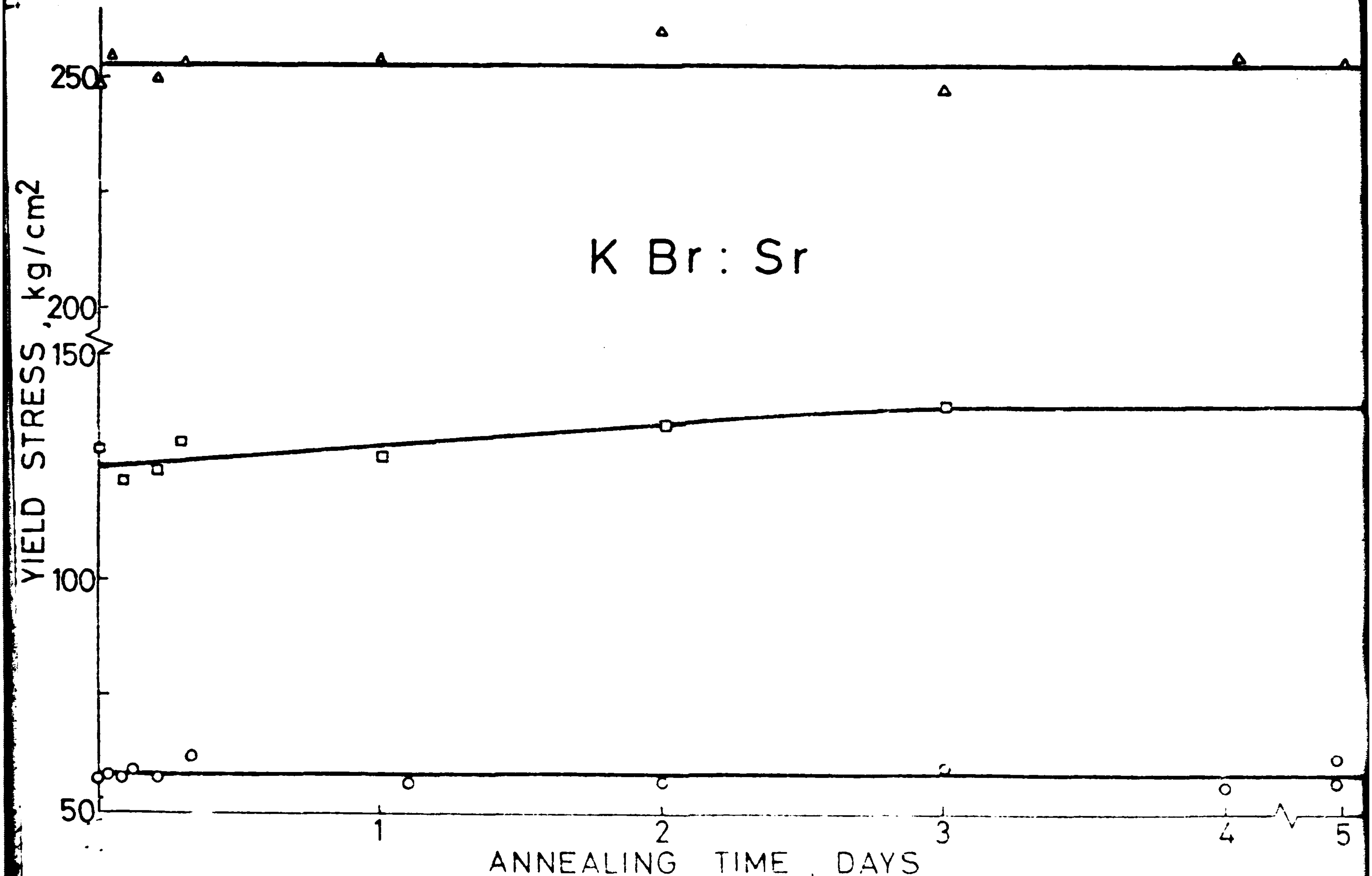
K Br : Sr
YIELD STRESS, kg/cm2
250
200
150
100
50
1
2
3
4
5
ANNEALING TIME, DAYS

FIG. 26

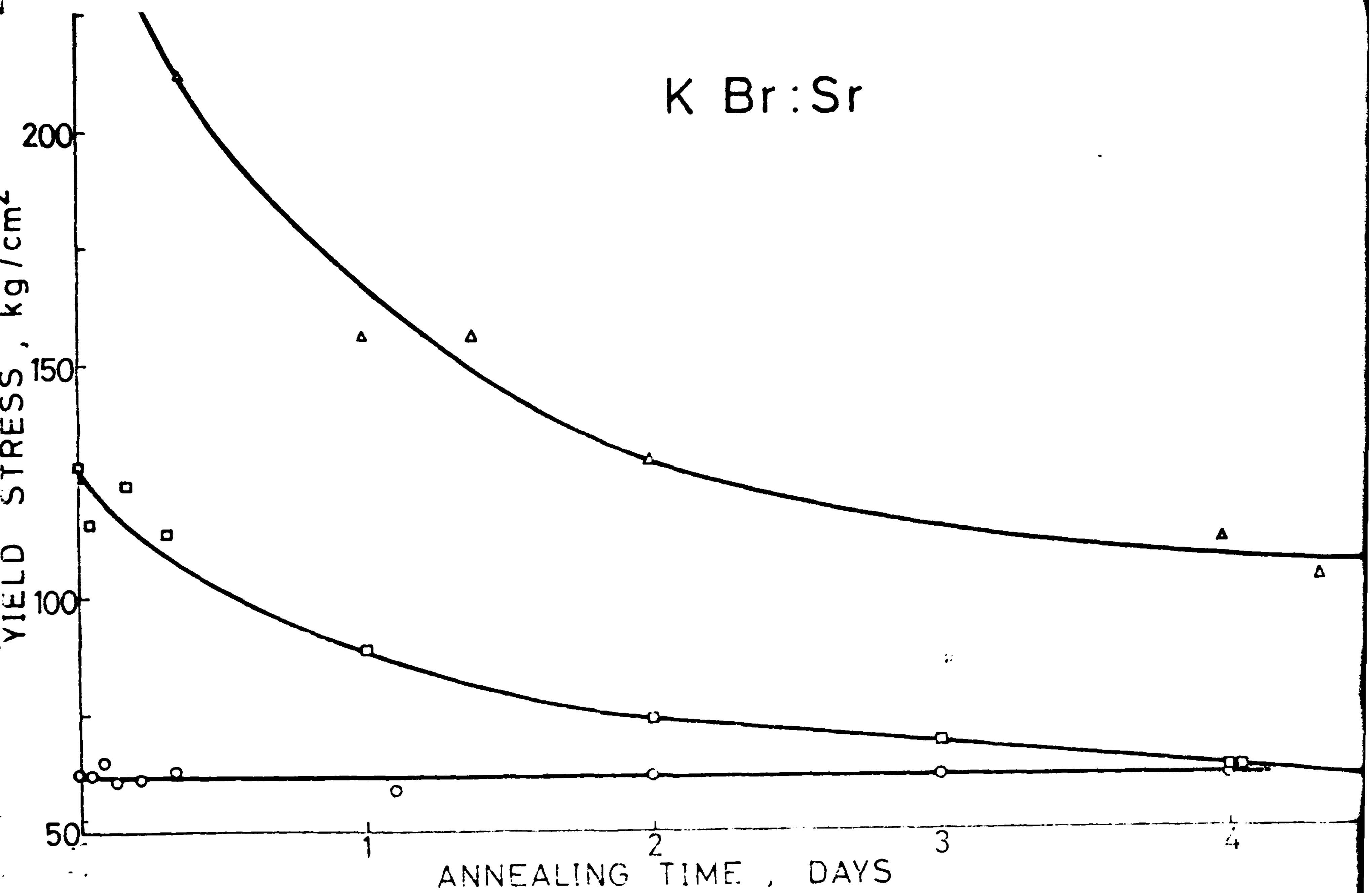
K Br : Sr
YIELD STRESS, kg/cm²
200
150
100
50
1
2
3
4
ANNEALING TIME, DAYS

FIG. 27

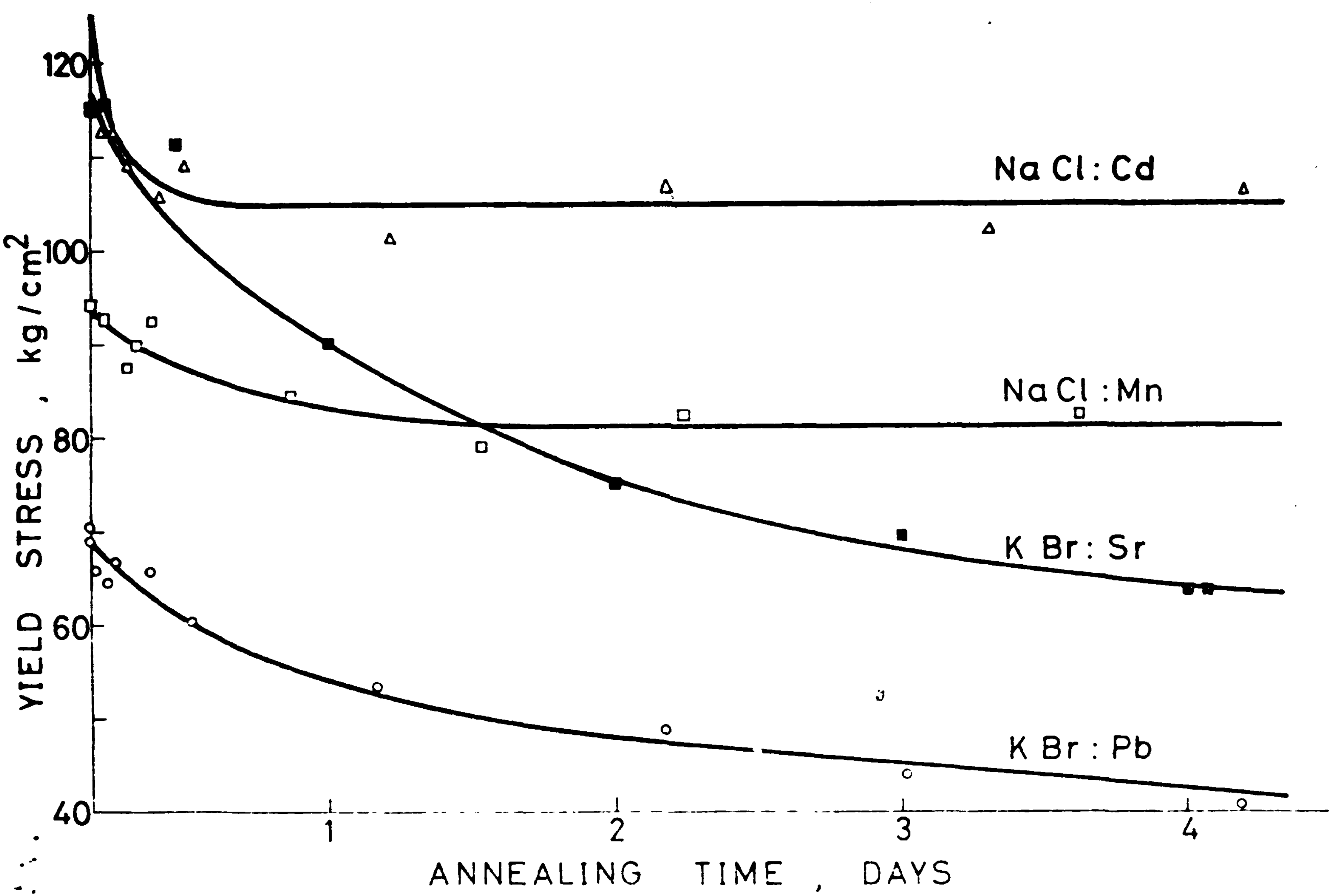

Na Cl : Cd
Na Cl : Mn
K Br : Sr
K Br : Pb
120
100
80
60
40
YIELD STRESS , kg/cm2
1
2
3
4
ANNEALING TIME , DAYS

FIG. 28

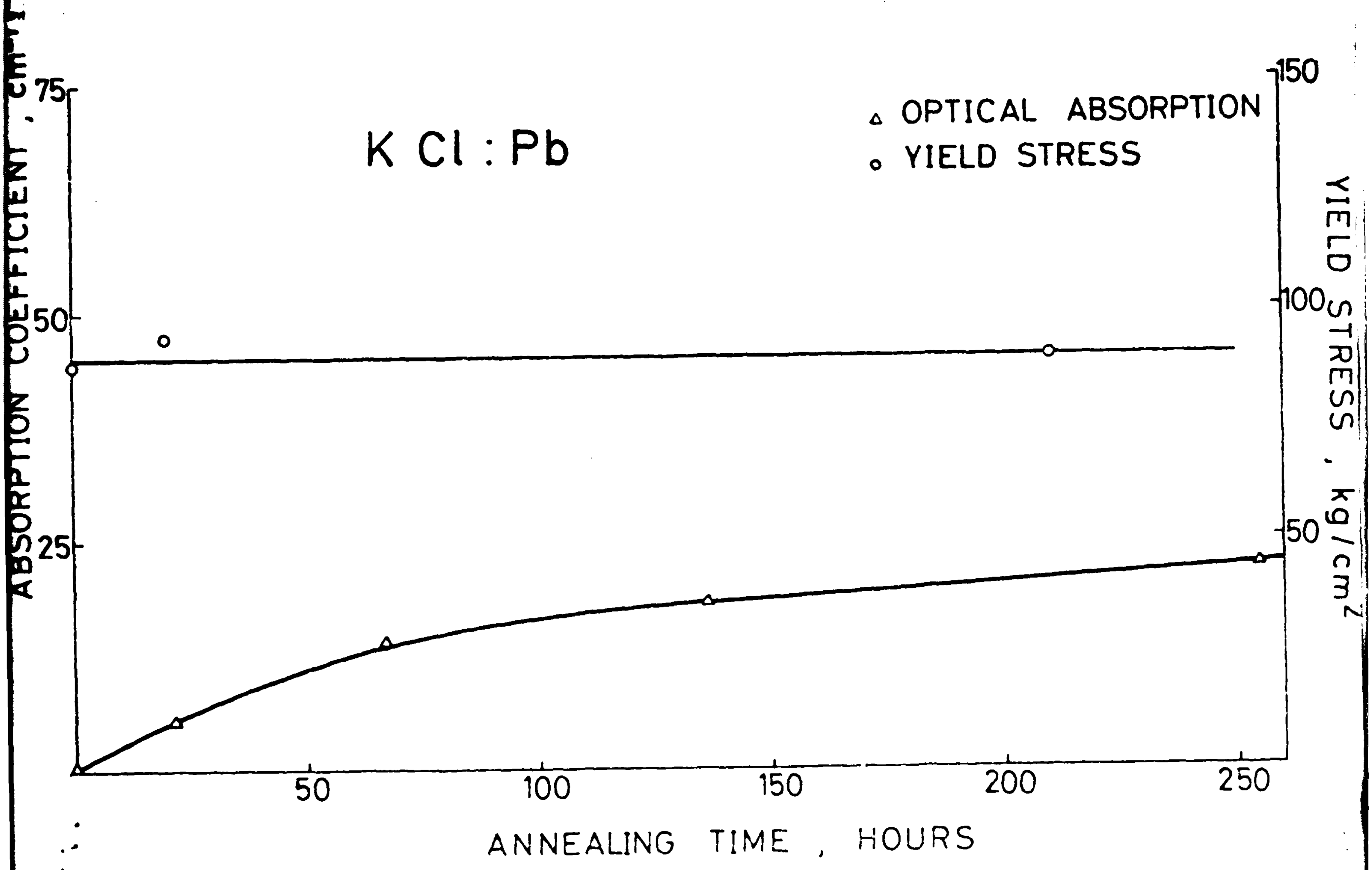
K Cl : Pb
OPTICAL ABSORPTION
YIELD STRESS
ABSORPTION COEFFICIENT , cm-1
YIELD STRESS , kg/cm2
75
50
25
150
100
50
50
100
150
200
250
ANNEALING TIME , HOURS

FIG. 29

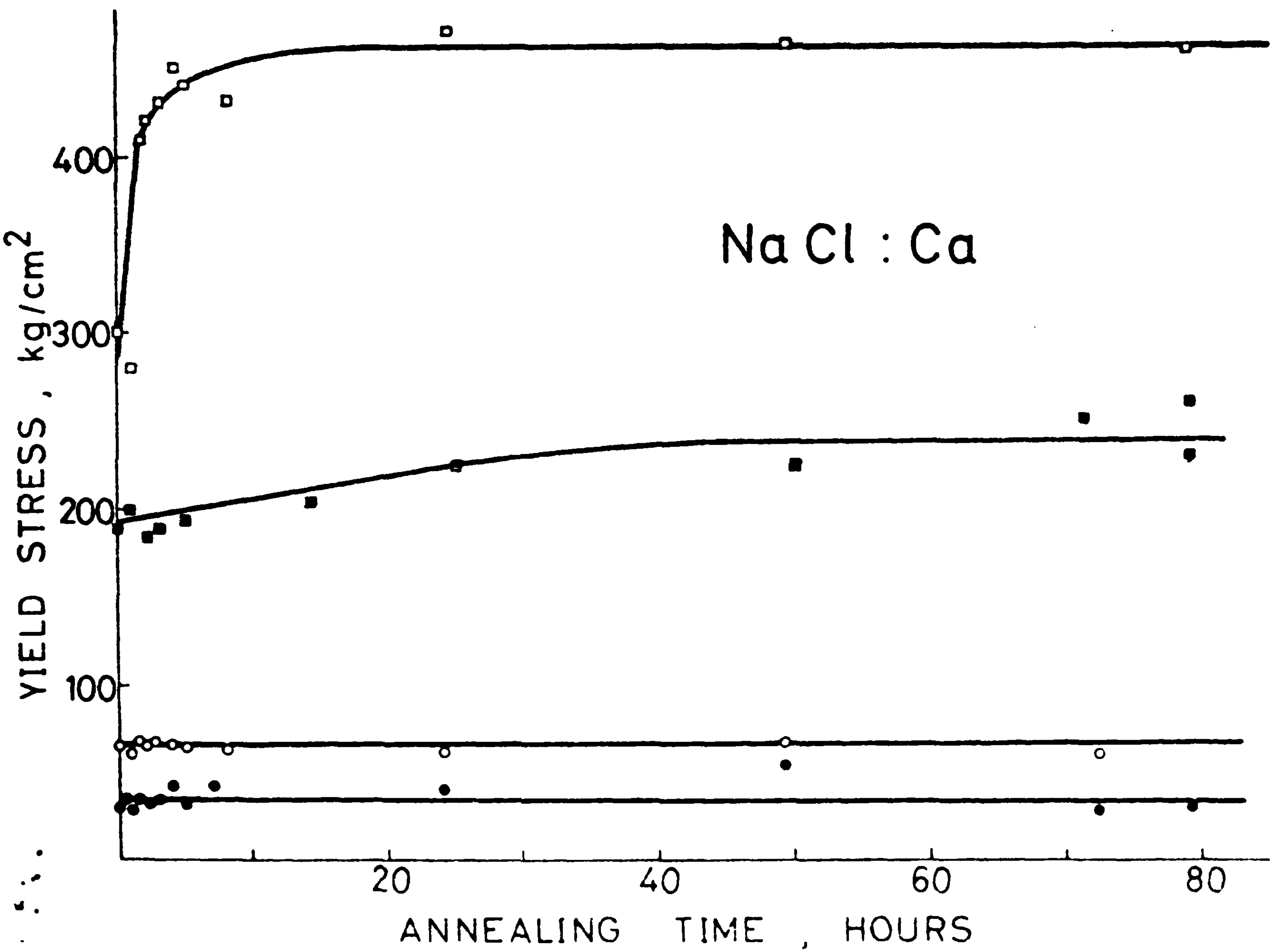
Na Cl : Ca
YIELD STRESS , kg/cm2
400
300
200
100
20
40
60
80
ANNEALING TIME , HOURS

FIG. 30

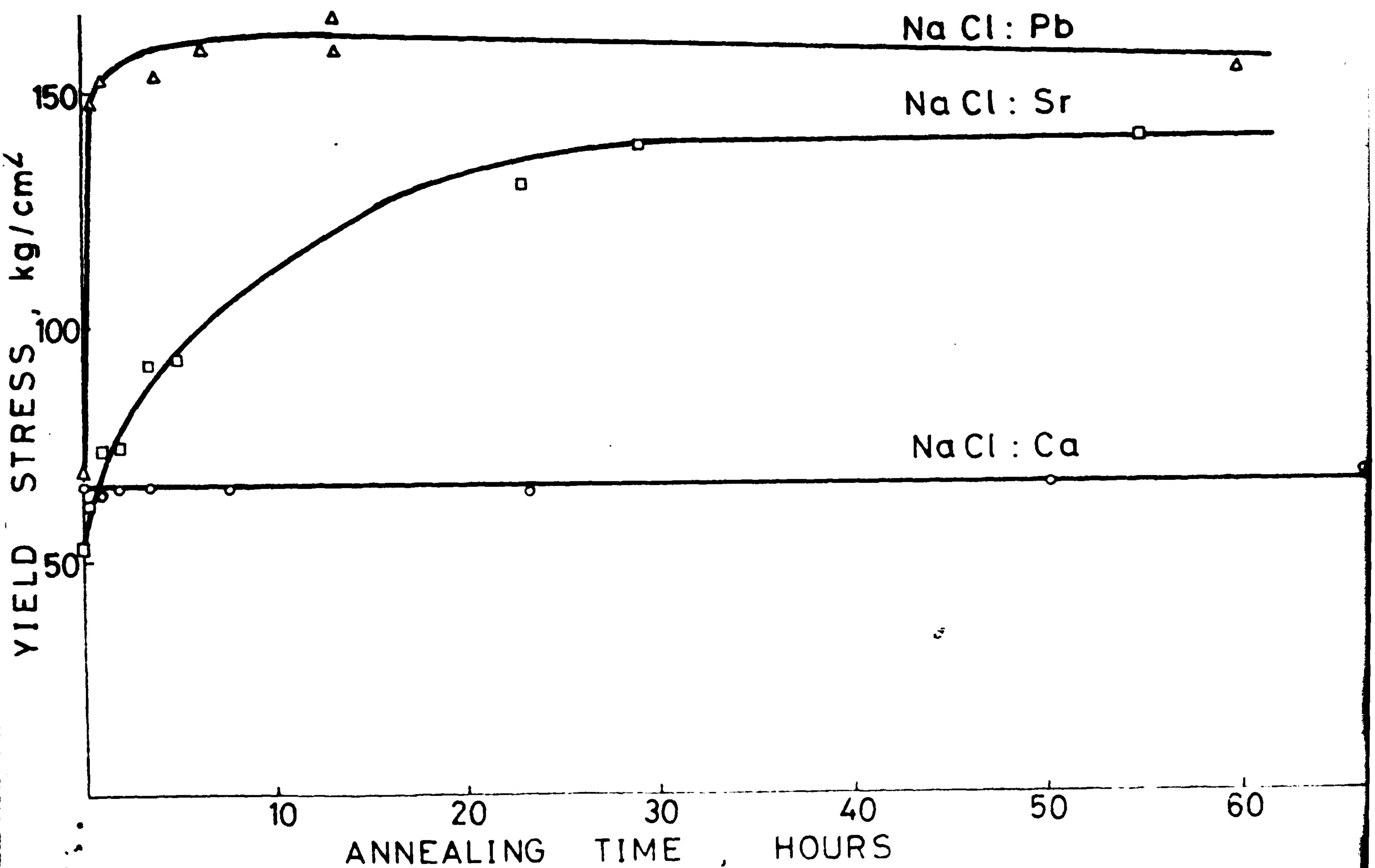
NaCl : Pb
NaCl : Sr
NaCl : Ca
YIELD STRESS, kg/cm²
150
100
50
10
20
30
40
50
60
ANNEALING TIME, HOURS

FIG. 31

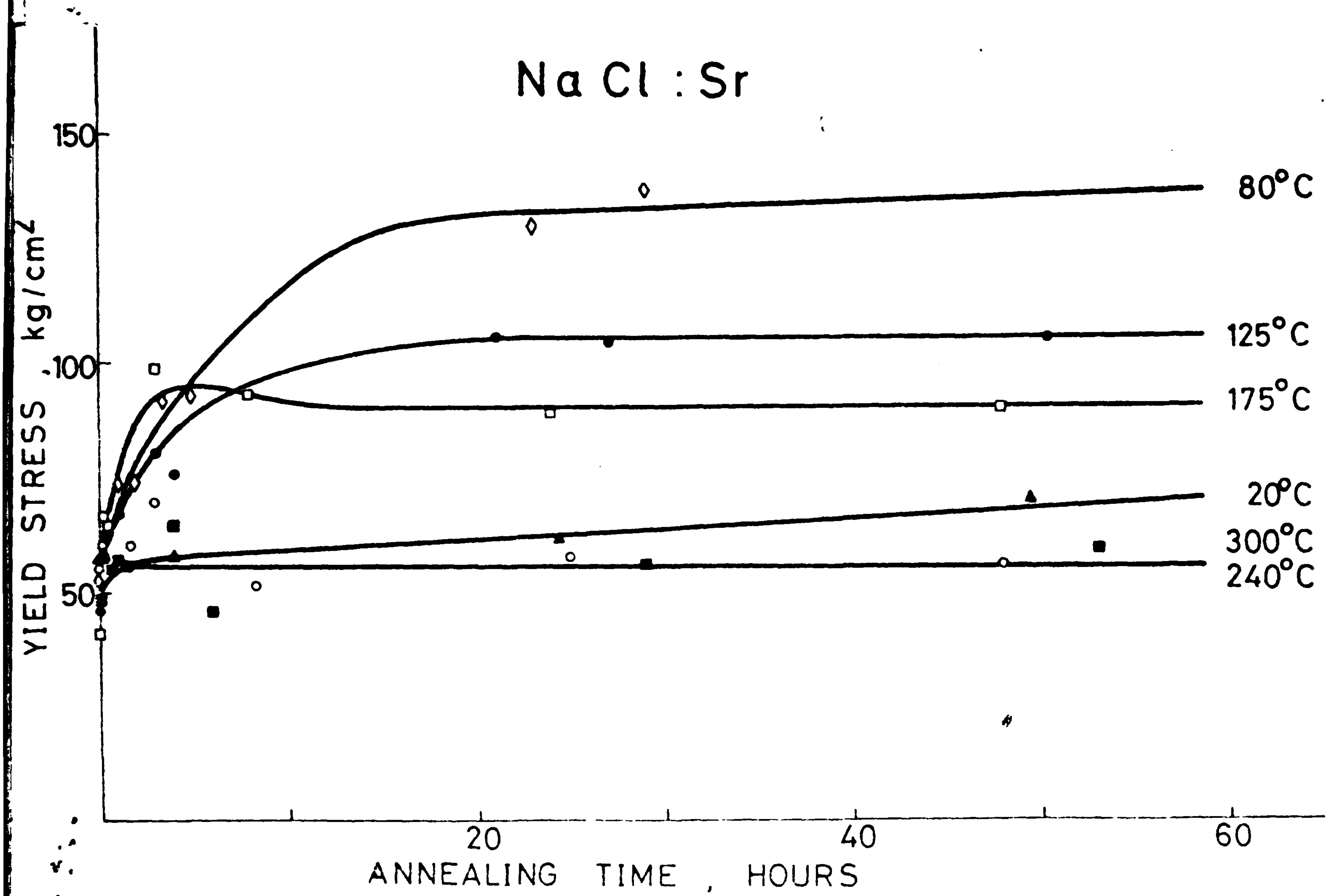

Na Cl : Sr
150
100
50
YIELD STRESS kg/cm²
80°C
125°C
175°C
20°C
300°C
240°C
20
40
60
ANNEALING TIME , HOURS

FIG. 32

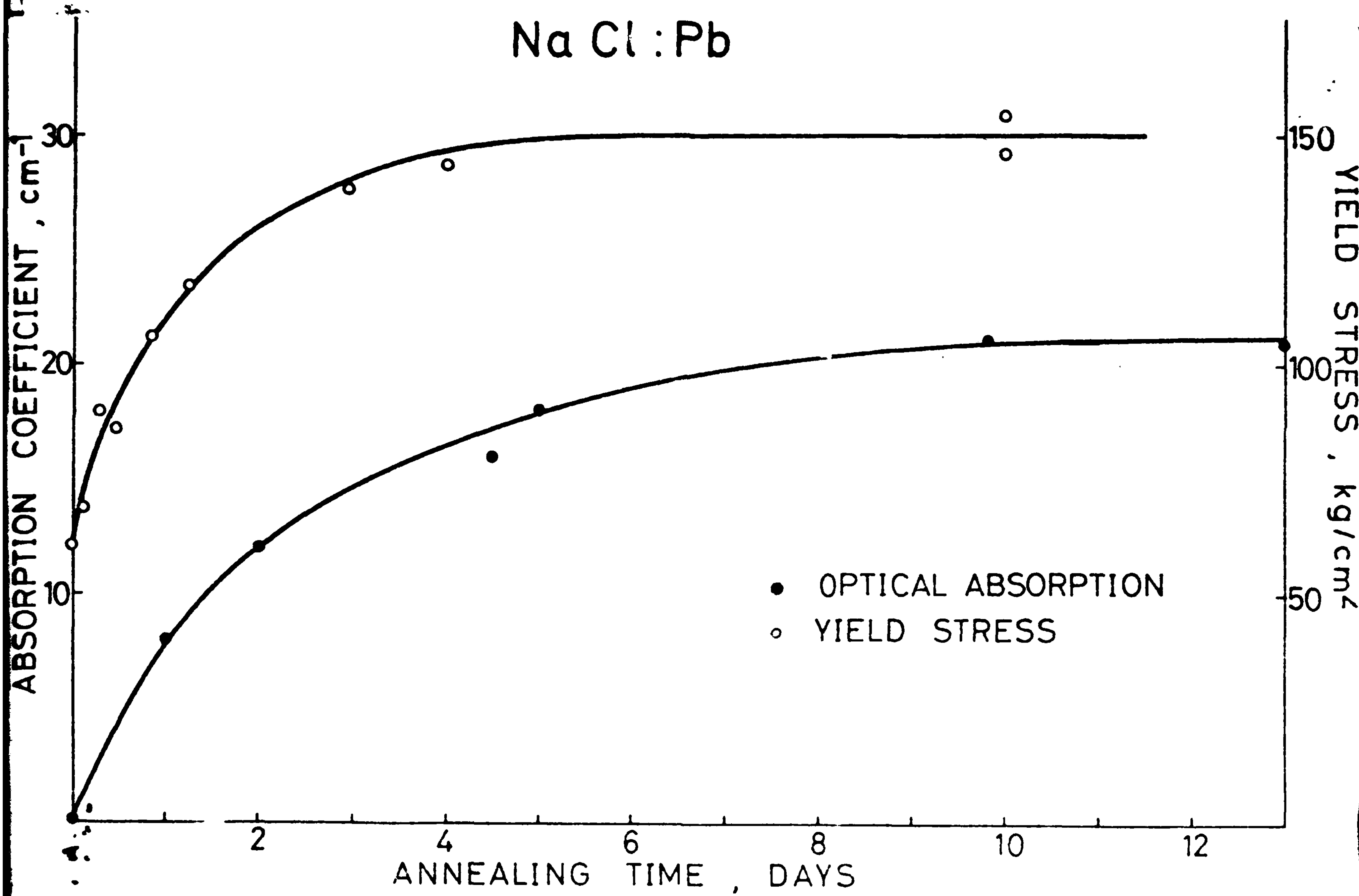

Na Cl : Pb
ABSORPTION COEFFICIENT , cm-1
YIELD STRESS , kg/cm2
OPTICAL ABSORPTION
YIELD STRESS
ANNEALING TIME , DAYS
10
20
30
50
100
150
2
4
6
8
10
12

FIG. 33

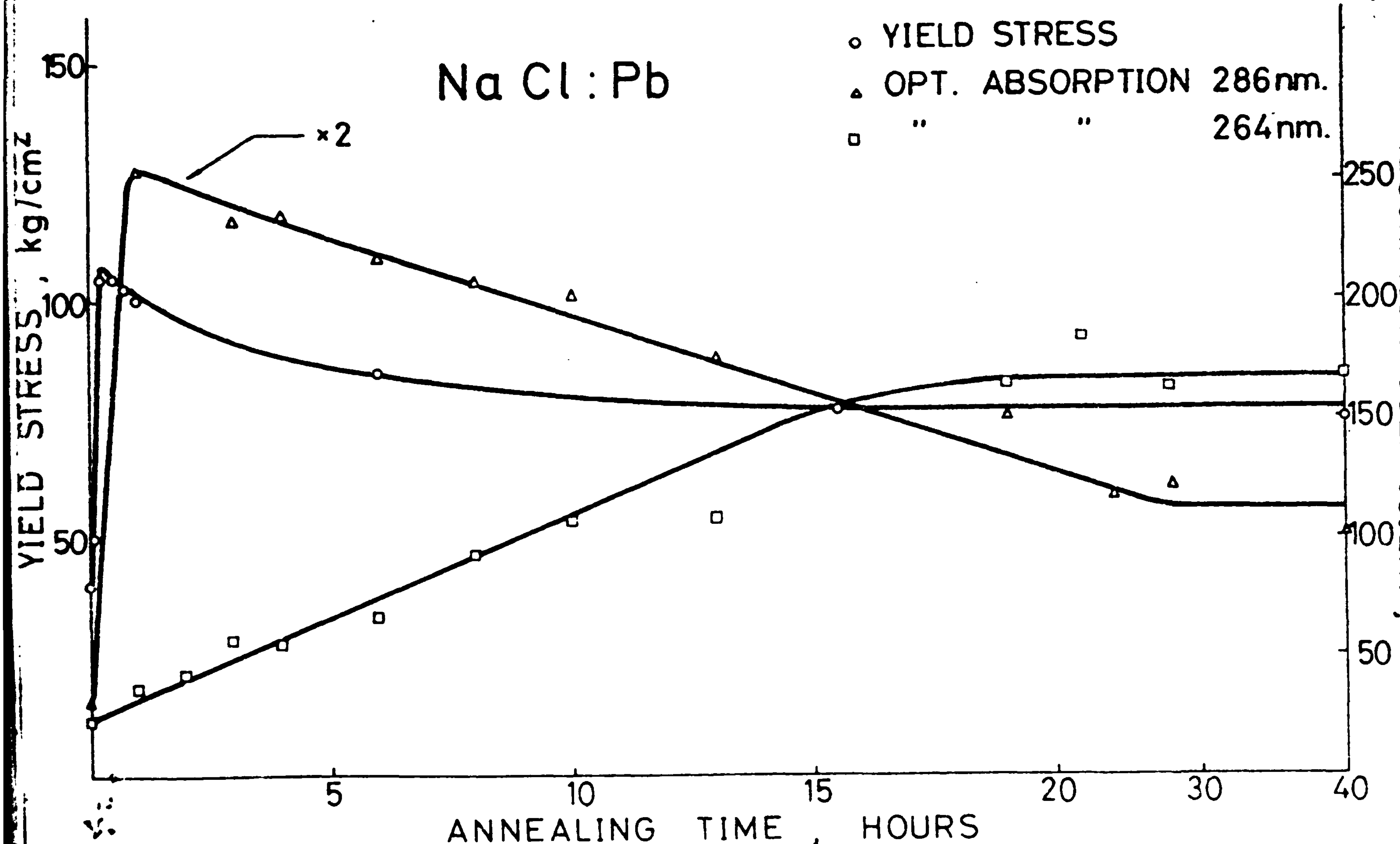
Na Cl : Pb
YIELD STRESS
OPT. ABSORPTION 286nm.
" " 264nm.
×2
150
100
50
250
200
150
100
50
YIELD STRESS , kg/cm²
5
10
15
20
30
40
ANNEALING TIME , HOURS
FIG. 34

DAT
ILM